

**FABRICATION AND CHARACTERIZATION OF
SILICON NITRIDE NANOPORES**

by

DHRUTI MAYUR TRIVEDI

B.A.Sc., University of British Columbia, 2004

A THESIS SUBMITTED IN PARTIAL FULFILLMENT OF THE
REQUIREMENTS FOR THE DEGREE OF

MASTER OF APPLIED SCIENCE

in

The Faculty of Graduate Studies
(Electrical and Computer Engineering)

THE UNIVERSITY OF BRITISH COLUMBIA

(Vancouver)

April 2009

© Dhruti Mayur Trivedi, 2009

ABSTRACT

The fabrication of synthetic nanopores with dimensional and electrical properties similar to organic alpha-hemolysin (α -HL) nanopores is required for the development of a novel genotyping device. This thesis details the development of synthetic nanopores with diameters below 5 nm fabricated by sputtering a free standing silicon nitride membrane using a tightly focused electron beam. Nanometer control is achieved with sputtering rates of 0.5 – 0.75 nm/s. This technique is further extended to fabricate a proof-of-concept array of 44 sub-5 nm nanopores in a single membrane to enable the detection of unamplified genomic DNA with acceptable signal-to-noise.

As-drilled inorganic nanopores have inferior electrical characteristics compared to α -HL. Careful study, however, revealed electrical noise sources that could be effectively reduced by chemical pretreatment of the pores and surface coating with poly-di-methyl-siloxane (PDMS). The chemical pretreatment targeted 1/f noise, while the PDMS reduced dielectric noise with an overall reduction in RMS current noise by a factor of 10. This resulted in processed nanopores with extremely favorable noise characteristics. These low noise silicon nitride nanopores were used to demonstrate single-molecule DNA translocation and probe capture with exceptional signal-to-noise ratios ranging from 40 – 150.

TABLE OF CONTENTS

ABSTRACT	ii
TABLE OF CONTENTS	iii
LIST OF TABLES.....	v
LIST OF FIGURES	vi
ACKNOWLEDGEMENTS	xi
DEDICATION	xiv
CHAPTER 1 INTRODUCTION	1
1.1 Nanopore Force Spectroscopy	3
1.2 Practical Implementation of Nanopore Force Spectroscopy	6
CHAPTER 2 NANOPORE CHIP FABRICATION.....	11
2.1 Synthetic Nanopore Membrane	12
2.2 Nanopore Fabrication	15
2.2.1 Background	15
2.2.2 Transmission Electron Microscope.....	18
2.2.3 Fabrication of Nanopores	24
2.3 Nanopore Arrays.....	31
CHAPTER 3 EXPERIMENTAL SETUP.....	37
CHAPTER 4 CHARACTERIZATION OF SYNTHETIC NANOPORES	43
CHAPTER 5 NOISE ANALYSIS AND REDUCTION IN SYNTHETIC NANOPORES	49
5.1 Noise Analysis at Zero Bias	52
5.1.1 Thermal Noise	53
5.1.2 Dielectric Noise.....	54
5.2 Noise Analysis under Bias	57

5.2.1 Shot Noise	58
5.2.2 1/f Noise	59
5.3 Methods to Reduce Noise.....	60
5.3.1 Reduction of Dielectric Noise.....	61
5.3.2 Reduction of 1/f Noise	66
CHAPTER 6 SYNTHETIC NANOPORE PERFORMANCE USING DNA.....	70
CHAPTER 7 CONCLUSION	75
BIBLIOGRAPHY	78
APPENDIX A: SIGNAL-TO-NOISE RATIO SCALES WITH THE NUMBER OF NANOPORES.....	83
APPENDIX B: DIMENSIONED DRAWINGS.....	86
B.1 Nanopore Cell	86
B.2 Cell Housing Assembly.....	88

LIST OF TABLES

Table 2.1: User controlled parameters on the FEI Tecnai™ G ² TEM that affects the current density at the sample.	22
Table 5.1: Numerical values determined from fitting the PSD to Eq. (5.1). The large difference in terms a_2 and a_3 arise due to the difference in dielectric properties of the Si _x N _y /Si chip and α -HL.	56
Table 5.2: Numerical values determined by fitting the PSD data sets using Eq. (5.1).	66

LIST OF FIGURES

Figure 1.1: Diagram showing the presence of a single nucleotide polymorphism (SNP) compared to a reference sequence.	2
Figure 1.2: Cross-section schematic view of (a) a transmembrane protein channel, α -HL, self-assembled in a phospholipid bilayer (b) a synthetic nanopore fabricated in a silicon nitride thin film membrane.	4
Figure 1.3: (a) A single α -HL nanopore incorporated into a lipid bilayer that separates the probe molecule from the analyte. The arrow on the side of each picture shows the direction of the force. Upon probe capture, the unblocked nanopore current of ~ 200 pA drops to ~ 50 pA (b), where the probe is free to hybridize to the analyte. (c) The potential is reduced to +10 mV to check for unsuccessful hybridization. Current noise observed is dominated by the capacitance of the lipid membrane. With successful hybridization, a -60 mV potential is applied to force the DNA duplex apart (d). After a time t_{off} the duplex dissociates and the associated open channel current at -60 mV is observed [12].	5
Figure 2.1: Cross-sectional schematic of a free standing membrane where t is the thickness of the membrane, w is the window size; h and l are the height and width of the supporting substrate, respectively.	12
Figure 2.2: Optical images showing the front and back side of a Si_xN_y TEM grid. The back side of the chip is recognizable by a Si etch pit. In relation to Figure 2.1, here, $h = 200 \mu\text{m}$, $l = 2.65 \text{ mm}$, $w = 50 \mu\text{m}$ and $t = 30 \text{ nm}$	15
Figure 2.3: A diagram of the electron beam as it passes through the electromagnetic lenses of a TEM. The sample sits in between the C2 condenser lens and the objective lens. The user views the sample image projected on the fluorescent pad.	19

Figure 2.4: Diagram showing the electron beam passing through the C2 lens that has a variable user controlled focal length. The rays show how the change in focal length changes the area of exposure on the membrane. The green ray line is focused on the membrane, giving the maximum current density required for nanopore drilling. 26

Figure 2.5: (a) shows the beam on the high resolution fluorescent pad just prior to commencing nanopore drilling (not yet reached the cross over point) (b) The cross over point is seen as the brightest spot in the figure. Here both pictures are taken at the same magnification and the diameters are comparable. (a) Has elliptical diameters of ~12 nm x 9 nm and (b) has elliptical diameters of ~10 nm x 7 nm. The crossover point has a diameter of < 2 nm. 27

Figure 2.6: A nanopore as seen on the fluorescent screen when the image is (a) under focused (b) at focus and (c) over focused. The circular Fresnel fringe is seen indicating an edge. This fringe is light when the image is under focused on the pad and dark when the image is over focused. The image is in focus at the point of minimum contrast as seen in (b). 29

Figure 2.7: Examples of nanopores with varying diameters demonstrating nanometer control using the TEM drilling technique. 30

Figure 2.8: A 3 x 3 array of ~5 nm nanopores with a pitch of 5 μm. Since the pitch is 1000 times the dimension of the nanopore, each individual nanopore picture has been stitched together to help visualize the array. Scale bar is 5 nm. 32

Figure 2.9: Cross-section diagram showing the FIB created pits in the SiN membrane. The pitch and the pit diameter are user controlled. 33

Figure 2.10: (a), (b), (c): A nanopore-in-pit array to showing a single 4 nm nanopore in (d). 44 nanopores were drilled in the TEM in two hours. 34

Figure 3.1: Synthetic nanopore experimental setup where the nanopore chip separates the two chambers of the electrochemical cell and the nanopore cell is housed in a Faraday cage. The electrodes are attached to a computer controlled patch clamp amplifier..... 38

Figure 3.2: Gold coated synthetic nanopore housing assembly showing the nanopore cell with the clamped electrodes connected to the amplifier head stage. A gold coated aluminium cover (not shown here) sits over top of the electrodes against the clamping plate to complete the Faraday cage..... 39

Figure 3.3: (a) Synthetic nanopore cell showing the two piece clamping assembly with the nanopore chip sandwiched in between two gaskets. (b) Top view of the assembly showing the position of the nanopore chip and gaskets (blue) between the two chambers of the electrochemical cell (red). The third chamber is engineered with future work in mind such as variable temperature experiments. 40

Figure 4.1: IV graph for a 3 nm nanopore (inset) over an applied voltage of -200 mV to 200 mV. 45

Figure 4.2: Model of double cone nanopore geometry where a TEM image would only show the narrowest diameter d_{tip} , the widest part of the nanopore d_{base} , is generally assumed to be at the surface of the membrane. The height h of the conical structure is 30 nm. 46

Figure 4.3: (a) Diagram showing the nanopore profile with dimensions calculated assuming a double cone model using the 2D TEM image and the measured conductance of the nanopore from Figure 4.1. The associated electric field profile for the double cone (b) structure helps visualize the force seen by a DNA strand within the nanopore. The region of highest field (red) is located at the narrowest constriction. 48

Figure 5.1: Four open pore current traces (100 ms long) at a 200 mV applied bias with low 1/f and low dielectric noise (a), with high dielectric noise (b), with high 1/f noise (c) and with both high dielectric

and 1/f noise (d). The resistance of the different nanopores was 300 – 400 MΩ. 51

Figure 5.2: The PSD of a Si_xN_y/Si chip and that of α-HL is fitted to Eq. (5.1) to determine the three coefficients. The hashed lines are the thermal noise given the resistance (~40 MΩ, ~1 GΩ) of the nanopores at room temperature..... 56

Figure 5.3: The PSD of a Si_xN_y/Si chip at zero bias and at 200 mV. The 1/f noise is dominant at low frequency..... 58

Figure 5.4: Cross-section diagram of the two silicone gaskets and the nanopore chip assembly. When there is no clamping pressure on the assembly (a), the silicone gaskets sit comfortably on the nanopore chip. Once the assembly is subjected to a clamping force (b), the poor adhesion of the gaskets results in the electrolyte seeping under the gaskets up to the seal contour created by the PTFE cell..... 62

Figure 5.5: (a) Optical top view image of a PDMS coated nanopore chip showing the PDMS close to the freestanding membrane window (b) Cross-section of PDMS painted nanopore chip (not to scale) 63

Figure 5.6: (a) Current vs. time (sampled at 100 kHz with a 10 kHz low pass Bessel filter) traces at zero bias for a bare Si_xN_y/Si nanopore chip (black), PDMS coated chip (blue) and that of α-HL (red). (b) PSD showing the effect of PDMS on the noise spectrum (here the PDMS data is split at 800 Hz). All three data sets are fit to Eq. (5.1) and their numerical values are tabulated in Table 5.2. The dashed lines are the thermal noise limit for the three nanopores with resistance of ~40 MΩ, ~100 MΩ and ~1 GΩ for bare Si_xN_y/Si, PDMS coated and α-HL, respectively. 65

Figure 5.7: (a) PSD for an untreated nanopore (black), a nanopore subjected to only 1/f noise reduction (grey), a nanopore subjected to both 1/f and dielectric noise reduction (blue) and α-HL (red) at 200 mV applied voltage. Blue dotted line represents the shot noise and

thermal noise limit for the full noise reduction treated nanopore (b)
RMS current noise for the same nanopore data sets..... 68

Figure 6.1: (a) Current blockade events for lambda-DNA at 150 mV bias.
Current is filtered at 10 kHz and sampled at 100 kHz. The inset shows
the possible configurations that the DNA takes during translocation.
(b) Histogram of the current level sampled in a 10 μ s time window
revealing the quantized current blockade levels representing the
translocation of dsDNA through the nanopore. 71

Figure 6.2: Single probe capture and escape event showing the
corresponding ionic current flow (black trace) through the nanopore at
a given voltage (blue solid line) and in the presence or absence of the
probe molecule. The inset shows (i) the open state (ii) the probe
captured state and (iii) the probe escaped open state. 73

ACKNOWLEDGEMENTS

From start to finish, there have been individuals who have gone out of their way to help me with this thesis. To you all, I remain forever grateful.

Foremost on this list is Dr. Andre Marziali, who has supported me even before I applied to graduate school. He has always taken the time to answer my questions and concerns, congratulated me on my successes and encouraged me through my failures. On a broader note, his hard work and dedication to university research and education are truly inspiring.

I would also like to express my gratitude to Dr. Karen Cheung who took up the challenge of supporting my graduate school application. Her guidance, expertise and research insight has steered me away from potential pitfalls. I will always remember her encouraging words throughout the thesis writing process.

My passion for micro- and nano-fabrication would not have existed if it was not for Dr. Mario Beaudoin and Dr. Andras Pattantyus-Abraham. Their patience, exceptional skill, attention to detail and often their sarcastic humour have influenced me in ways they may never know. I hope I can some day do the same for another misguided, short, brown, female undergraduate student.

Dr. Li Yang, who is the Nano-Imaging Facility Manager at Simon Fraser University, and Mary Fletcher, who is the Senior Technician with the Department of Metals and Materials Engineering at the

University of British Columbia, have provided training and assistance on the transmission electron microscope, focused ion beam and scanning electron microscope. They have on several occasions helped me meet deadlines by overriding equipment usage time and suggesting techniques and settings for optimal results. I appreciate all their special attention and trust when using equipment outside of regular working hours.

Among my colleagues in the lab, I can not leave out the contribution of Dr. Vincent Tabard-Cossa. He performed both the DNA translocation and probe capture experiments along with diligently collecting the data used for nanopore noise analysis. The success of this work has been magnified by his curiosity, observation, logical thinking, hard work and motivation. These admirable qualities of his I hope to emulate throughout my career.

During the thesis writing process, there were times when my patience and confidence in myself was wearing thin. It was in these dark moments that the encouragement and guidance of Dr. Jason Dwyer pushed me through. His positive and constructive feedback in all aspects of my work has made an everlasting impression on me. Words are not enough to express my gratitude.

I can not forget the contribution made by specific former and current lab-mates, such as Dr. Jon Nakane, who first looked into the development of the synthetic nanopores; Dr. Robin Coope, who very kindly helped edit this thesis, Matt Wiggin, who has always patiently answered all my questions and Nahid Jetha, for all his technical

assistance, moral support and encouragement. The rest of the Applied Biophysics Lab must be acknowledged for all their technical, scientific and administrative assistance. I will miss their sarcasm and wit.

The support and encouragement I have received from those mentioned above dims in comparison to that received from my family and friends. I will always be indebted to Chris Tong, Julia Ko and Dr. Vishakha Monga for everything that they have done. I can only hope and pray for their health and prosperity.

My parents and my sister have always been by my side even if I have not been by theirs. This unconditional support I know I have for the rest of my life. To them, I dedicate this thesis.

To Pappa,

for always believing in me...

To Mummy,

for your faith and Raviwars (Sunday fasts)...

To my sister, Vatsi,

for your undying love, support and humour...

CHAPTER 1 INTRODUCTION

The twenty-first century has seen an increasing interest in providing more targeted health care (personalized medicine) based on the genetic makeup of an individual (genotype). Personalized medicine holds the promise of improved patient outcome, reduced cost, and reduced adverse drug reactions. There is, however, much still to be done in understanding genetic factors in disease and treatment response, and in the development of robust and cost effective analysis devices. The latter challenge is the subject of this work.

The vast majority of the genome (all the DNA) of humans is identical from person to person. Natural variation between humans is largely in the form of single nucleotide polymorphisms (SNPs): single base pair changes at specific sites on the DNA sequence, as seen in Figure 1.1. Clinically, these SNPs can be linked to an individual's disease development [1], response to pathogens [2], predisposition to developing chronic illnesses [1, 3, 4], or drug efficacy [4, 5]. The latter is of great interest to both the public and pharmaceutical companies, as genotype information can both decrease the cost of clinical trials by restricting the size of patient cohorts, and improves the efficacy of treatments. The challenge for a clinical genotyping device is to be able to provide data on a wide variety of SNP tests in a robust and rapid manner, with as little user involvement as possible.

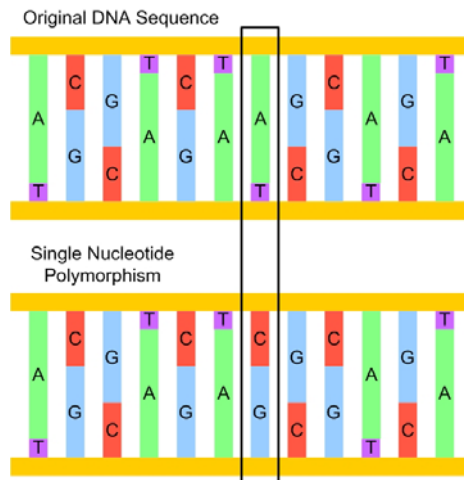


Figure 1.1: Diagram showing the presence of a single nucleotide polymorphism (SNP) compared to a reference sequence.

The personalized approach is currently utilized in only a small number of circumstances, where administering a drug to persons with known non-compatible genotype can lead to therapeutic failure, toxic reactions or even death [5]. The expensive chemotherapy drug Herceptin, for example, is effective for only those breast cancer patients who exhibit an over-expression of the HER2 receptor [6, 7]. Another example is that of variations found in the cytochrome P450 enzyme family that determine drug metabolism rates among patients, which in turn dictates the drug dosage a patient receives [5].

Current genotyping devices require expensive and time consuming steps such as sample amplification, purification and fluorescent labelling to achieve acceptable signal-to-noise. Minimal sample

preparation and the development of a label free detection technique would increase the speed of the tests leading to improved adoption and better patient care.

Over the last few years, nanopore force spectroscopy has emerged as a technique for the detection and analysis of bio-molecules, in particular DNA. This electronic detection approach has the potential to be a rapid, label free diagnostic test requiring minimal to no amplification.

1.1 Nanopore Force Spectroscopy

A nanopore is a nanometer-sized hole in a thin membrane such as the hole formed by the transmembrane protein channel alpha-hemolysin (α -HL) or a pore fabricated in a synthetic thin film. Figure 1.2 shows a cross-sectional schematic of an α -HL nanopore in a phospholipid bilayer (a) and a synthetic nanopore fabricated in a silicon nitride membrane (b). Under an applied bias, electrolyte ions pass through the open nanopore giving a stable “open pore” current. Charged polymers, such as DNA can be made to pass through (translocate) under an applied potential. During translocation, the DNA strand blocks the passage of ions resulting in a measurable change in the nanopore current, called a current blockade.

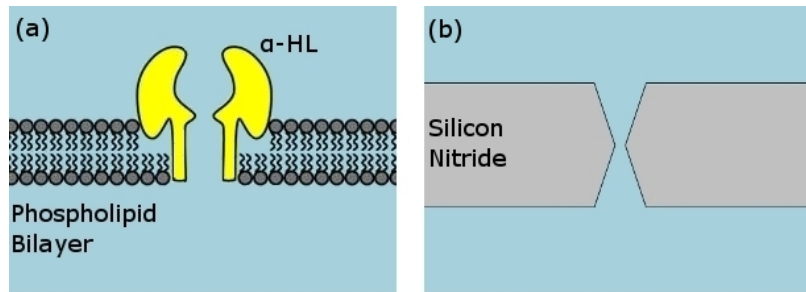


Figure 1.2: Cross-section schematic view of (a) a transmembrane protein channel, α -HL, self-assembled in a phospholipid bilayer (b) a synthetic nanopore fabricated in a silicon nitride thin film membrane.

Single stranded DNA (ssDNA) has a hydrodynamic diameter of ~ 1.4 nm [8] while double stranded DNA (dsDNA) has a hydrodynamic diameter of ~ 2 nm [9]. The limiting aperture of α -HL, ~ 1.5 nm [10] in diameter, can be used to discriminate against dsDNA while allowing ssDNA to pass through. Due to this discrimination, α -HL can be used to dissociate DNA duplexes by attempting to translocate the duplex through the pore under an applied pulling force. In this mode the time taken to force apart the hybridized duplex at a given voltage (dissociation time), can be used to calculate its binding energy. Variations in binding energy can be correlated to SNPs in the analyte sequence.

Figure 1.3 shows the voltage (red) and current trace (blue) during a single force spectroscopy event. A biotinylated ssDNA probe is covalently anchored to an avidin protein (~ 5 nm in diameter) [11] at one end, to prevent the ssDNA from translocating through the

nanopore under an applied bias. There is a drop in current (Figure 1.3 (b)) when the probe inserts itself into the nanopore (probe capture). The un-anchored end of the ssDNA probe is free to probe for complementary ssDNA on the other side of the membrane (Figure 1.3 (c)).

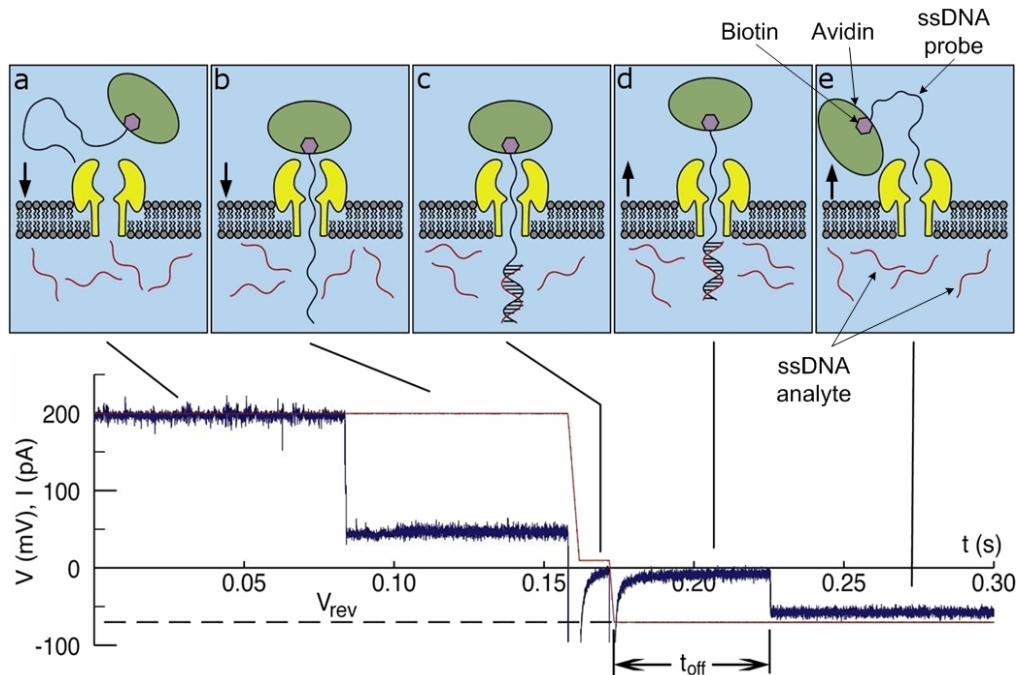


Figure 1.3: (a) A single α -HL nanopore incorporated into a lipid bilayer that separates the probe molecule from the analyte. The arrow on the side of each picture shows the direction of the force. Upon probe capture, the unblocked nanopore current of ~ 200 pA drops to ~ 50 pA (b), where the probe is free to hybridize to the analyte. (c) The potential is reduced to +10 mV to check for unsuccessful hybridization. Current noise observed is dominated by the capacitance of the lipid membrane. With successful hybridization, a -60 mV potential is applied to force the DNA duplex apart (d). After a time t_{off} the duplex dissociates and the associated open channel current at -60 mV is observed [12].

Under reverse potential, the ssDNA probe is pulled from the nanopore (Figure 1.3 (d)). The force exerted eventually leads to duplex dissociation. Real time current recording captures the dissociation time (t_{off}) of this duplex at the given applied voltage. The dissociated probe is driven away by the electric field, bringing the current back to an open pore current value proportional to the applied voltage (Figure 1.3 (e)).

Dissociation times for a single probe-analyte species are recorded at varying potentials to extract an energy landscape for that specific species. The quantitative parameters are different for a perfect complement (one half of the Watson-Crick pair) analyte compared to an analyte with a single nucleotide polymorphism (SNP) making this detection technique highly sensitive. Nanopore force spectroscopy as described above was successfully demonstrated in 2004 using a single α -HL nanopore in a lipid bilayer [12].

1.2 Practical Implementation of Nanopore Force Spectroscopy

Clinical genotyping requires the collection and analysis of statistically significant force spectroscopy data. Recording large amounts of data on a single α -HL nanopore can be time consuming and consequently such data collection is more favourably carried out using multiple nanopores on the same membrane. By increasing the number of

nanopores on the membrane, it is also possible to achieve useful signal-to-noise while sampling lower concentrations of analyte. This means that sample amplification can be greatly reduced or even eliminated with a sufficiently large number of nanopores while still maintaining acceptable signal-to-noise (See Appendix A for calculations). This motivation led to the successful demonstration of nanopore force spectroscopy on multiple α -HL nanopores (at least 100 nanopores) in 2007 [13].

Nanopore force spectroscopy is a purely electrical detection technique for single molecule analysis and offers a number of advantages. The lack of fluorescent labelling eliminates reagents, labelling steps, and optical detection instrumentation. The single molecule sensitivity reduces or eliminates, the need for sample amplification, reducing the cost and time of sample preparation. However, the α -HL platform has a few limitations that make it difficult to incorporate in a commercial genotyping device. Due to natural aging, the lipid bilayer supporting the α -HL nanopore is stable for a limited time period (< 24 hrs) [14] and it is not very robust when exposed to mechanical movement and user handling. The pores are also stable over a small range of operational conditions such as pH (6 – 9) and applied voltage (< \pm 400 mV) [15]. In addition to this, the organic platform is not as compatible with current semiconductor fabrication and micro fluidic technology.

Were it possible to realize a nanopore with all the advantages of the α -HL system but with greater reliability, the nanopore approach to genotyping would become viable. A nanopore in an electrically insulating synthetic membrane would be mechanically robust, potentially capable of larger bias voltages and compatible with current semiconductor and micro fluidic fabrication.

Direct fabrication of nanometer sized holes less than 5 nm in synthetic membranes is a challenging task and is still beyond the 5 nm to 10 nm achievable with electron beam lithography [16, 17]. Non-standard techniques have been developed to craft sub-5 nm nanopores in a variety of membranes. This decade has seen several groups develop sub-5 nm nanopores on different membrane materials such as silicon dioxide [18-20], silicon nitride (Si_xN_y)¹ [18, 20-25] and metals [26, 27] by fabricating a hole with a diameter larger than 10 nm and then shrinking the size of this larger nanopore using an electron beam [19, 20, 22-25, 27], ion beam [18, 21, 22, 26] or material deposition [28, 29]. Other techniques such as feed back controlled chemical etching have also been explored on silicon [30], polyimide [31] and poly ethylene terephthalate [32]. The first sub-5 nm nanopore was fabricated in 2001

¹ Although the molecular formula for silicon nitride is Si_3N_4 , low stress silicon nitride is used to fabricate free standing membranes and is non-stoichiometric. Si_xN_y is used in order to accommodate all non-stoichiometric forms of the compound.

by reducing the diameter of a 60 nm nanopore in Si_xN_y to less than 2 nm using a custom made ion beam irradiation system [21].

This thesis describes the direct fabrication sub-5 nm nanopores by exposing a silicon nitride membrane to an electron beam in a transmission electron microscope (TEM). Nanopores with diameters below 5 nm are directly fabricated, and not by shrinking a larger nanopore. They are created by a sputtering effect where high energy electrons dislodge surface atoms leading to a loss of material and the eventual formation of a hole in the membrane (TEM drilling technique) as detailed in Chapter 2. This chapter also details the successful extension of this work into the fabrication of an array of sub-5 nm nanopores as a proof-of-concept. To the best of the author's knowledge this is the first demonstration of a sub-5 nm array of nanopores on a single synthetic membrane using the TEM drilling technique. Chapter 3 discusses the prototype instrument design and system integration for these nanopore chips.

Unlike α -HL, the three dimensional (3D) geometry of Si_xN_y nanopores can vary from nanopore to nanopore. Meller et al. have recently shown that a silicon nitride nanopore created using the TEM drilling technique has an 'hour glass' structure [24]. As discussed in Chapter 4 the conductance of the nanopore was used to gain insight into the pore geometry by assuming a specific 3D model.

Nanopores developed in our lab initially showed poor electrical characteristics compared to α -HL, as did those developed elsewhere [28, 29, 33]. Noise exceeded any current signal from DNA translocation events. Fortunately, however, sensitivity of the noise to nanopore and membrane parameters enabled the noise itself to be systematically investigated and reduced. The dielectric nature of the synthetic nanopore material and its interactions with the ionic electrolyte [22] were a major source of noise on the current signal. Power spectral density (PSD) plots were used to differentiate two dominant independent sources of noise – dielectric noise and $1/f$ noise, providing a basis for the reduction of this noise by two orders of magnitude. Chapter 5 details the observation, analysis and reduction techniques used to create low noise synthetic nanopores while Chapter 6 describes DNA translocation and avidin-anchored DNA probe capture experiments carried out to test the performance of these nanopores.

The development of a synthetic nanopore chip, associated instrumentation design, analysis and improvement of the signal quality together with successful translocation and probe capture experiments is the first step to engineering a useful, clinical genotyping device using the synthetic nanopore platform. This thesis describes novel work enabling the fabrication of electrically quiet synthetic pores suitable for incorporation in such a device.

CHAPTER 2 NANOPORE CHIP FABRICATION

In the DNA measurement scheme proposed in this thesis, the nanopore serves as the only ionic pathway between the two reservoirs of an electrochemical cell. The nanopore can be self-assembled in a lipid bilayer (organic nanopore) or fabricated in a synthetic membrane (synthetic nanopore).

Proteinaceous α -HL is one of the more successfully used organic nanopores in biosensing. It is a protein channel that self assembles to form a nanopore in a single lipid bilayer ~ 10 nm thick, with a 1.5 nm constriction at its limiting aperture. As discussed in Chapter 1, the α -HL platform has a few disadvantages for applications in clinical genotyping technology such as poor mechanical robustness, short lifetimes, a small range of stable operating conditions and low compatibility with current semiconductor fabrication and lab on chip technologies. A synthetic nanopore platform has the potential to address all these limitations. Additionally, a synthetic nanopore is not limited to a specific size, aiding the investigation of different bio-molecules using force spectroscopy.

The synthetic nanopore developed in our lab is fabricated using a tightly focused beam of electrons in a transmission electron

microscope (TEM), where the beam is used to ablate atoms from the surface of a free standing silicon nitride membrane. This chapter details the selection criteria for the freestanding membrane, the fabrication of a nanopore on the membrane using a TEM and the development of nanopore arrays.

2.1 Synthetic Nanopore Membrane

The ideal membrane for nanopores is tens of nanometers thick, electrically insulating and easy to manufacture. Silicon nitride is a standard nanofabrication material that meets these criteria.

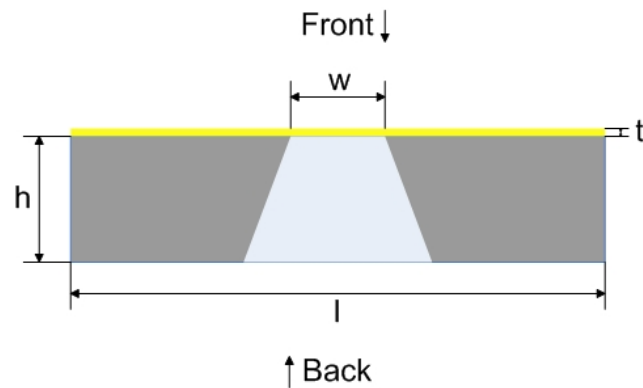


Figure 2.1: Cross-sectional schematic of a free standing membrane where t is the thickness of the membrane, w is the window size; h and l are the height and width of the supporting substrate, respectively.

Figure 2.1 shows a schematic of a free standing membrane with thickness (t), window size (w), substrate width (l) and height (h). An

electron beam produced by a TEM is used to fabricate the nanopores in the membrane. The use of the TEM as a fabrication tool places limits on the size of the nanopore substrate. We use commercially available Si_xN_y membranes; TEM grids used to support loose samples for TEM imaging, from Structure Probe Inc, although a variety of vendors produce similar products. The membrane is low-stress Si_xN_y and the substrate material is crystalline silicon ($\text{Si}_x\text{N}_y/\text{Si}$ chip).

The length of the probe molecule and the desired magnitude of the current blockade influence the choice of the membrane thickness. For simplicity we assume a cylindrical geometry, where the length of the nanopore is equal to the thickness of the membrane. For force spectroscopy, the probe molecule must be able to interact with the analyte on the other side of the membrane. Therefore, the length of the probe must be greater than the thickness of the membrane. However, there are restrictions on the maximum length of a ssDNA probe that can be chemically synthesized. Single stranded DNA of ~ 200 nucleotides (nt) can be synthesized with sufficient purity and concentration [34]. This translates to a maximum probe length of 90 nm ($1\text{nt} = 4.5 \text{ \AA}$) [8] for ssDNA and hence the thickness of the membrane must be less than 90 nm. Eqs. (2.1) and (2.2) show this relationship derived from Ohm's law and the resistance of a cylindrical pore [35].

$$\frac{\Delta I}{I_{open}} = \frac{\Delta A_{DNA}}{A_{pore}} \quad (2.1)$$

$$\Delta I = \frac{\kappa V \Delta A_{DNA}}{L_{pore}} \quad (2.2)$$

The current blockade (ΔI) is inversely proportional to the length of the nanopore (L_{pore}), implying that a thinner membrane gives a larger current blockade for a given voltage (V), conductivity (κ) and cross-sectional area of the DNA strand (ΔA_{DNA}). The inverse relationship between the membrane thickness and the current blockade further motivates our need for sub-90 nm membranes. Commercially, 20 nm and 30 nm membranes are available with a membrane window size of 50 μm x 50 μm from Structure Probe Inc. The 20 nm membranes were found to be fragile and prone to breakage under an intense electron beam (possibly due to thermal effects). Therefore, TEM grids produced by Structure probe Inc. with a window size of 50 μm x 50 μm and a membrane thickness of 30 nm (Figure 2.2) were best suited for our purposes.

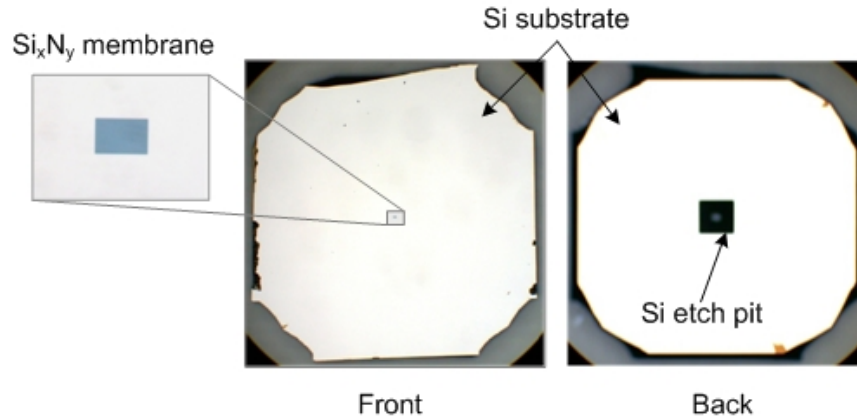


Figure 2.2: Optical images showing the front and back side of a Si_xN_y TEM grid. The back side of the chip is recognizable by a Si etch pit. In relation to Figure 2.1, here, $h = 200 \mu\text{m}$, $l = 2.65 \text{ mm}$, $w = 50 \mu\text{m}$ and $t = 30 \text{ nm}$.

2.2 Nanopore Fabrication

Direct drilling of a nanopore to the desired diameter with a TEM was first demonstrated by Storm et al. in a silicon dioxide membrane [19]. Since then, this technique has been adopted by several groups [20, 22-24, 35]. This section describes the theoretical background and the TEM parameters that affect nanopore formation.

2.2.1 Background

TEM-drilled nanopores are created by a sputtering process, where atoms are ejected from the surface of the membrane by high energy electrons. Sputtering occurs for incident electron energies that exceed a threshold value determined by the binding energy of the surface

atom. The binding energy is the minimum energy required to free the atom from the membrane surface. The threshold incident electron energy (E_{th}) is calculated using Eq. (2.3) for an atom with atomic mass number (A) and binding energy (E_b) [36].

$$E_b = (E_{th} / 465.7 A)(1.02 + E_{th} / 10^6) \quad (\text{eV}) \quad (2.3)$$

Therefore, the incident electron energy used in the TEM must be higher than E_{th} .

Another value of interest is the sputtering rate which is dependent on the sputtering cross-section. The sputtering cross-section is an effective area for collision for a given target material and at a given incident electron energy. The sputtering rate is defined by Eq. (2.4) [37],

$$S = (J / e)(\sigma)(t_m) \quad (\text{nm/s}) \quad (2.4)$$

where the sputtering rate (S) is dependent on the sputtering cross-section (σ in cm^2) for a target material at the chosen incident electron energy. The current density (J/e) is in electrons/ cm^2/s and (t_m) is the thickness of one monolayer of the target material in nanometers. Both the sputtering cross-sections and the threshold incident electron energy are tabulated for different elements [38]. Although these equations and tables were derived for electron bombardment on materials with a single atomic species, it can still be applied to

compounds like silicon nitride to estimate the incident electron energy required and the sputtering rate.

The physics of sputtering for multi-atomic materials by electron bombardment is not well understood but the idea of preferential sputtering exists, where a specific species of the compound is easier to sputter due to a lower binding energy or a more efficient energy transfer from the incident electrons [38]. This would imply that over time the multi-atomic surface is enriched by the species that was left behind. Groups have used electron energy loss spectroscopy (EELS) [20] and energy dispersive X-ray (EDX) [19] analysis to observe that exposure to a focused electron beam leaves a more silicated surface behind, implying that nitrogen would be preferentially sputtered for our membranes. Therefore, the limiting rate for the creation of nanopores is sputtering of silicon.

The maximum surface binding energy for silicon is 13 eV [38]. Using Eq. (2.3) we estimate a minimum incident electron energy of ~150 keV for silicon. In order to ensure that we were well above the estimated minimum range, an incident electron energy of 200 keV was used.

Atomic sputtering cross-sections for silicon at 200 keV are reported to be between 60 cm^2 to 270 cm^2 [38]. A minimum sputtering rate of 0.8 nm/s can be calculated using Eq. 2.4, with a current density of

10^4 A/cm². We will see later that the experimental sputtering rate seen is consistent with that predicted here. Section 2.2.2 describes how the current density and the incident electron energy influence nanopore fabrication in a TEM.

2.2.2 Transmission Electron Microscope

The specific TEM model used for nanopore fabrication is dependent on the capability of the TEM to produce the required electron energy and the current density. A TEM is equipped with an electron gun, which is the source of electrons, and with electromagnetic lenses that are used to focus the beam on the sample and project the image of the sample on a fluorescent screen. The sample is placed between the condenser lenses and the objective lenses as seen in Figure 2.3. Only those TEM user settings that affect sputtering are discussed in this subsection.

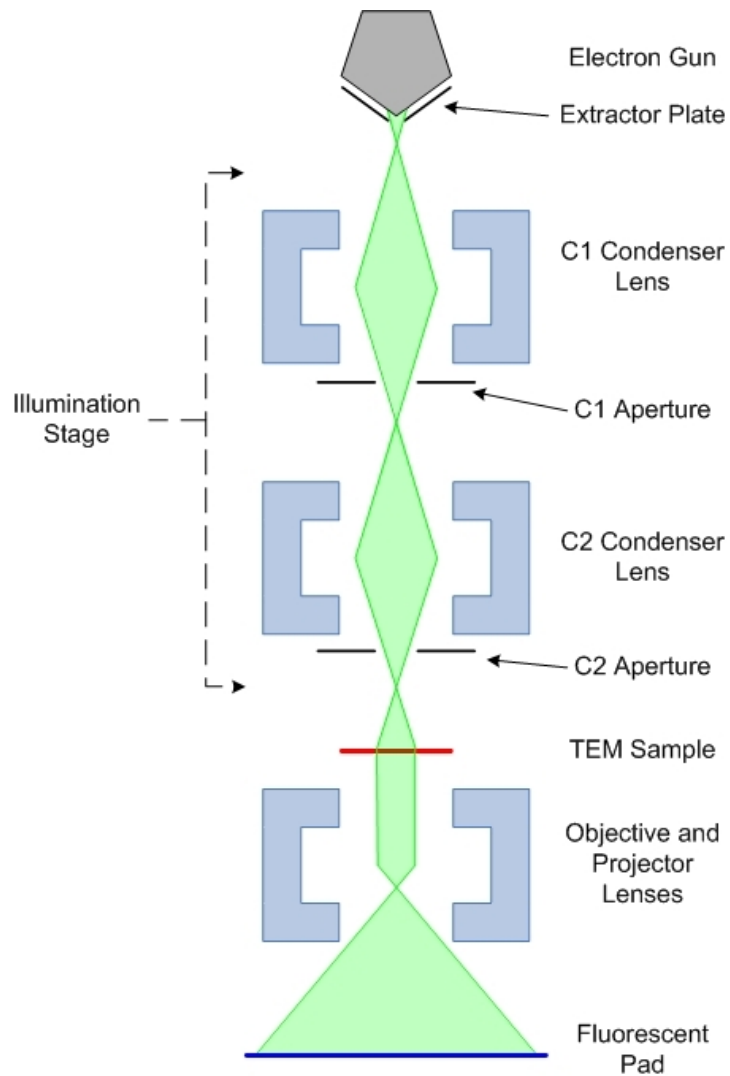


Figure 2.3: A diagram of the electron beam as it passes through the electromagnetic lenses of a TEM. The sample sits in between the C2 condenser lens and the objective lens. The user views the sample image projected on the fluorescent pad.

The electron gun provides a steady stream of electrons with the desired electron energy. As calculated in section 2.2.1, TEM models capable of incident electron energies greater than 150 keV are required for this work. Also, different electron gun designs are capable

of achieving different maximum current density values. Thermionic guns that use tungsten (W) or lanthanum hexa-boride (LaB_6) are capable of current densities on the order of 3 A/cm^2 and 100 A/cm^2 , respectively. The Schottky field emission gun and the cold field emission gun can both achieve current densities of up to 10^6 A/cm^2 . From section 2.2.1, achieving a minimum sputtering rate of 0.8 nm/s would require current densities in the 10^4 A/cm^2 range, implying that the thermionic gun and LaB_6 gun are poor candidates for nanopore formation in silicon nitride. The FEI Tecnai™ G² F20 TEM used in this project is equipped with a Schottky field emission gun which can achieve the required current density and incident electron energy of up to 200 keV [39, 40].

The field emission gun is a tungsten filament coated with a layer of zirconium oxide. An extractor plate located near the gun (Figure 2.3) provides a positive potential in the 2 kV to 7 kV range, to extract the electrons from the tip of the filament. The potential on the extractor plate is called the extractor voltage and sets the electron emission current which influences the sputtering rate. For our work an extraction voltage of $3800 \text{ V} - 4000 \text{ V}$ was used which corresponds to an electron emission current of $51 \text{ } \mu\text{A} - 54 \text{ } \mu\text{A}$ at the gun. Note that the current seen at the sample is much lower due to losses from the lenses and the apertures. For our setup this value is in the 10^{-10} A range.

The stream of electrons from the gun is then controlled by electromagnetic condenser lenses and associated condenser apertures. This is called the illumination stage (Figure 2.3) and helps create a collimated beam of electrons [41]. There are two condenser lenses C1 and C2 on the FEI Tecnai™ TEM. The former and its aperture set the diameter of the beam, called the spot size. The smaller the beam diameter the smaller the nanopore that one can drill given that the current density value is satisfied (discussed further in section 2.2.3). There are two modes on the TEM which define two different ranges for the beam diameter. The Microprobe mode is generally used for imaging and has beam diameters from approximately 25 nm to 1 nm. The Nanoprobe mode, which introduces new optics into the system in order to achieve a smaller beam diameter, is used for analysis and produces a beam diameter ranging from 2 nm to 0.2 nm. Our protocol uses the Nanoprobe setting with spot size 5, which translates to a numerical value of ~ 1.5 nm [40] and a current density larger than 100 A/cm^2 .

The second condenser lens called the C2 condenser lens has a variable focal length. The user can focus the beam onto the sample using the 'intensity' knob at a given C2 aperture. This adjustment of the focal length increases the current density of the beam at the sample plane increasing the sputtering rate. For the purpose of making nanopores it is important to have the maximum number of electrons (at spot size 5) reach the sample and hence the largest diameter is chosen for the C2 aperture [40].

When the beam hits a thin sample, electrons pass through the sample and create an image on a fluorescent screen through the objective and projection lenses. As visual feedback is used to determine whether a nanopore is created, the TEM image must also be optimized for best results. In our experience, optimal nanopore drilling and visual feedback were achieved at an objective magnification of 125,000x. The objective lens also has an objective aperture that controls the image contrast. A small aperture gives the best contrast but is more difficult to align and is sensitive to astigmatism (asymmetry in the lens). For nanopore fabrication, the largest objective aperture was used as the loss of image contrast was not observed to be significant and aided the user in achieving good alignment with minimum beam astigmatism.

Table 2.1: User controlled parameters on the FEI Tecnai™ G² TEM that affects the current density at the sample.

TEM Parameter	Setting
High Tension	200 keV
Extracting Voltage	3800 V – 4000 V
Condenser C1 Aperture	4
Condenser C2 Aperture	4
Objective Aperture	7
Spotsize	Nanoprobe 5
Magnification	125,000x

The TEM settings used to create the nanopores in this work are summarized in Table 2.1. Once these settings have been selected, electron beam alignment and astigmatism can be adjusted. The gun-tilt and gun-shift controls align the beam such that it comes down the optical axis of the TEM and is centered on the lenses and corresponding apertures ensuring that the maximum number of electrons reaches the sample.

The shape of the beam that hits the membrane affects the geometry of the nanopore. Astigmatism is caused by a change in the magnetization of the lenses every time it is adjusted or turned on and by acquired charge in the apertures near the lenses due to surface contamination [41]. Although the C1 lens remains at the same initial setting, the C2 lens and the objective lenses are constantly adjusted, leading to a drift in alignment and astigmatism in the beam over the course of hours.

Beam alignment and astigmatism are initially adjusted (coarse alignment) at a magnification below 26,000x and just prior to nanopore drilling (fine alignment) at 125,000x. Once these parameters have been optimized, the current seen at the sample is constant [40, 41].

2.2.3 Fabrication of Nanopores

The silicon nitride membrane described in section 2.1 is loaded into the TEM after initial coarse alignment. The electron beam is at a low magnification of 4400x and the beam is spread out to its lowest intensity to speed scanning of the substrate to locate the membrane window. The relative positions of the four corners of the membrane are measured using a built-in micrometer and the beam is centered on the membrane. The image is magnified to 125,000x for fine beam alignment. Fine beam alignment is repeated every time a sample is loaded.

Nanopore fabrication is dependent on the time of exposure to the beam and the current density. The user controls both parameters by adjusting the objective and C2 condenser. Proper visual feedback gives the user accurate control over the time of exposure to the beam. The objective lens is adjusted, by using the 'focus' knob, to focus the image of the membrane on the fluorescent pad below. In this case, the semi-transparent membrane shows small granular features at a magnification of 125,000x. Sample focus is defined by the point of minimum contrast, i.e. where the granular features disappear. Finding the point of minimum contrast is often difficult for the user but improves with practice. The membrane is set to the focused state prior to initiating the drilling process.

At this point, the beam exposes an area on the membrane, which is 10 – 15 nm in diameter. The current density is $\sim 100 \text{ A/cm}^2$ with an estimated sputtering rate of 1 pm/s. In order to increase the sputtering rate, the current density is increased (seen in Eq. (2.4)) by reducing the area of exposure. Altering the focal length of the condenser lens C2, by using the 'intensity' knob, widens and narrows the electron beam on the sample changing the area exposed. Figure 2.4 shows three ray traces after the electron beam passes through condenser lens C2. The red, blue and green ray lines each show different focal lengths of the C2 lens exposing a different circular area on the membrane resulting in different current densities.

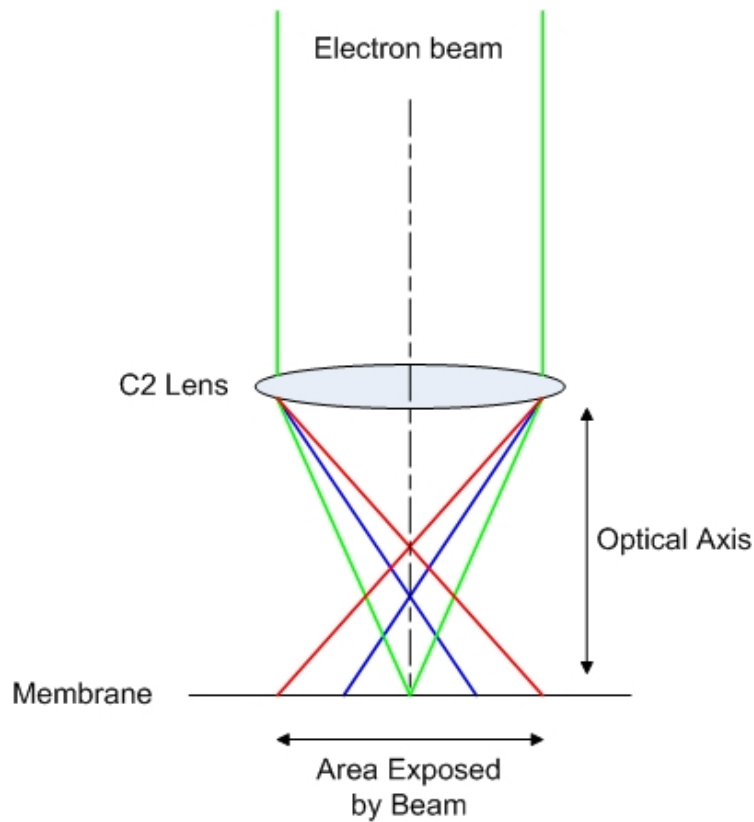


Figure 2.4: Diagram showing the electron beam passing through the C2 lens that has a variable user controlled focal length. The rays show how the change in focal length changes the area of exposure on the membrane. The green ray line is focused on the membrane, giving the maximum current density required for nanopore drilling.

Changing the focal length of the lens does not alter the beam current, implying that at the crossover point (green ray line), maximum current density is achieved. Under good beam alignment conditions, the diameter of the beam at the crossover point is 1 nm - 2 nm, as described in section 2.2.2, with a resulting current density of 10^4 A/cm².

Nanopore drilling begins at an appreciable rate once the beam is narrowed down to the point of cross over (by adjusting the C2 lens) as seen in Figure 2.5 (b). Visual evidence (drilling and imaging occur simultaneously) of sputtering from the membrane is observed at this point. The area between the crossover point and the edge of illumination displays a change in contrast. Darker rings appear to be flickering due to the presence of the beam. This flickering motion could be a result of the damaging sputtering action at the membrane site. The dark spots in Figure 2.5 are a degraded patch on the fluorescent pad due to excessive exposure over time to the focused electron beam.

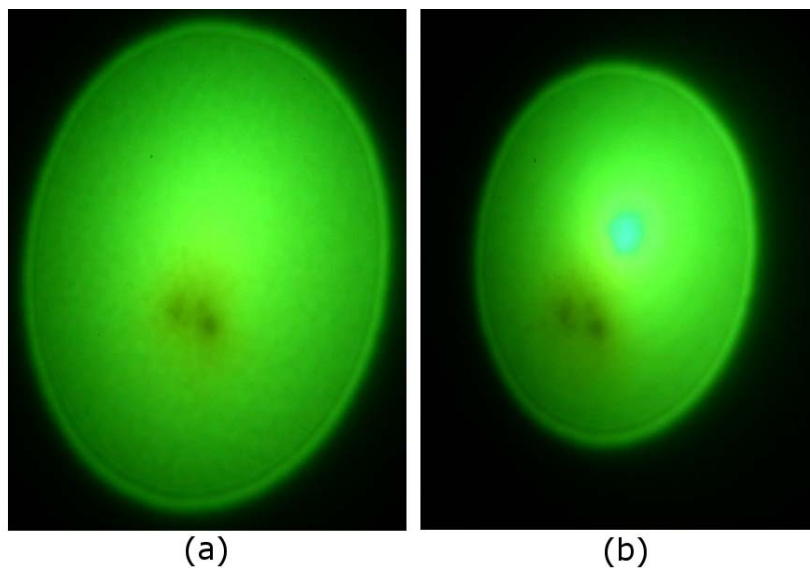


Figure 2.5: (a) shows the beam on the high resolution fluorescent pad just prior to commencing nanopore drilling (not yet reached the cross over point) (b) The cross over point is seen as the brightest spot in the figure. Here both pictures are taken at the same magnification and the diameters are comparable. (a) Has elliptical diameters of ~ 12 nm x 9 nm and (b) has elliptical diameters of ~ 10 nm x 7 nm. The crossover point has a diameter of < 2 nm.

In microscopy mode, an edge is observed due to the presence of Fresnel fringes. This diffraction effect appears as a dark or light circular ring near the edge of the feature when the image is 'over focused' or 'under focused', respectively. A nanopore is created when there is no more material left to sputter at the crossover point. The loss of material leads to the formation of an edge and a dark Fresnel fringe appears from the crossover point. There is significantly less flickering motion observed once this fringe appears possibly due to the reduction in sputtering. Figure 2.6 shows three images of a nanopore just after being created in the 'under focused' (Figure 2.6 (a)), 'at focus' (Figure 2.6 (b)) and 'over focused' (Figure 2.6 (c)) state. Once the fringe is observed, the electron beam is spread to a diameter of over 150 nm as seen on the fluorescent pad ($\sim 1.2 \mu\text{m}$ on the sample), lowering the current density and the sputtering rate by at least three orders of magnitude and effectively stopping the nanopore drilling process. The time taken to create a nanopore is measured as the time of exposure at the crossover point. The time of exposure ranges from 40 s to 60 s giving a sputtering rate of 0.75 nm/s to 0.5 nm/s, respectively. This is consistent with the estimated sputtering rate of 0.8 nm/s in section 2.2.1.

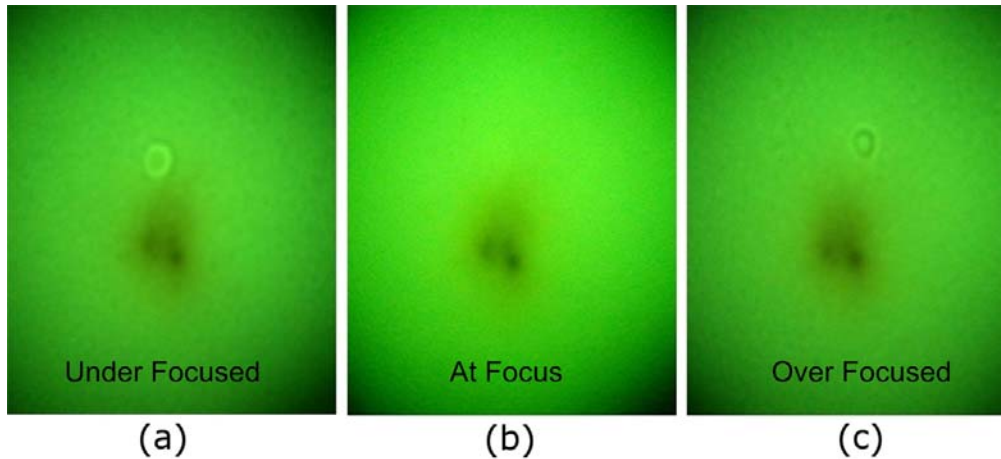
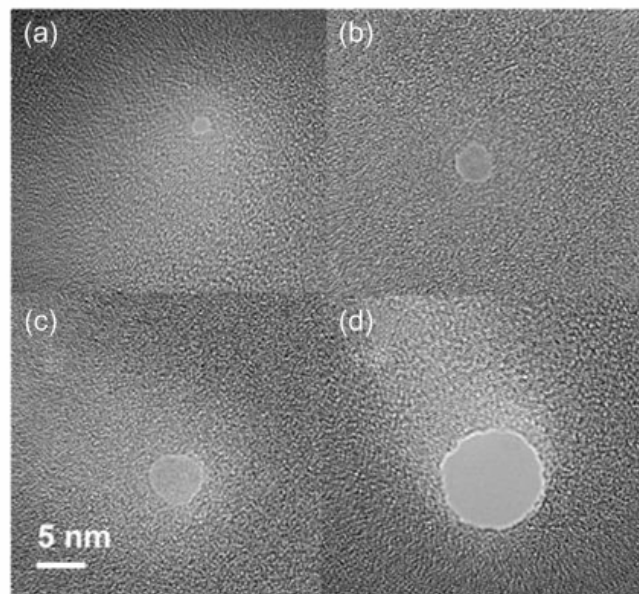


Figure 2.6: A nanopore as seen on the fluorescent screen when the image is (a) under focused (b) at focus and (c) over focused. The circular Fresnel fringe is seen indicating an edge. This fringe is light when the image is under focused on the pad and dark when the image is over focused on the pad. The image is in focus at the point of minimum contrast as seen in (b).

Note, that with further exposure to the crossover point the fringe continues to expand as the nanopore increases in diameter. The final diameter of the nanopore is dependent on the user's ability to observe the presence of the fringe. There is however, a lower limit to this observation of the fringe. The crossover point is extremely bright, as seen in Figure 2.5 (b) and makes it difficult for the user to distinguish a dark fringe under it. Using the settings described in section 2.2.2 and under good beam alignment, the cross over point is 1 nm - 2 nm in diameter. Therefore, the smallest nanopore that can be fabricated is ~2 nm.

Digital pictures of nanopores fabricated using the TEM drilling technique can be recorded using the same instrument and under the same beam settings. The current density, however, is kept orders of magnitude lower than while drilling. The Tecnai™ TEM is fitted with a Gatan Charge Coupled Device (CCD) camera to record images. Selecting a magnification for recording an image is left to the user's discretion. Note that the user must reduce astigmatism for the selected magnification for good image quality. A maximum magnification of 590,000x was used for our nanopores with minimum objective astigmatism. In microscopy, it is good practice to keep the image slightly under focused for maximum contrast. Figure 2.7 shows the characteristic light Fresnel fringe at the nanopore boundary for four different nanopores.



Nanopore size: (a) = 1.5 nm; (b) = 3.5 nm; (c) = 5 nm; (d) = 10 nm

Figure 2.7: Examples of nanopores with varying diameters demonstrating nanometer control using the TEM drilling technique.

2.3 Nanopore Arrays

As discussed in the introduction, there is a statistical advantage in using multiple nanopores to obtain data. This was demonstrated in other work using an array of over 100 α -HL nanopores on the same membrane [13]. There is also a clinical advantage to arrays, in that, an increase in the number of nanopores on a single membrane allows for the detection of lower concentrations of analyte with acceptable signal-to-noise (see Appendix A). This is significant for the development of a commercial genotyping device intended to be used with unamplified genomic DNA (~50 fM analyte concentration).

The current seen through a nanopore array scales with the number of nanopores eventually exceeding the measurement limits of the existing instrumentation. Therefore, a reduced array of nanopores, here 40 - 50 sub-5 nm nanopores was fabricated as a proof-of-concept. This reduced array would also test scaling of performance and signal-to-noise. It is important to note that an array of 40 - 50 nanopores is not sufficient for a commercial genotyping device which would need tens of thousands of nanopores on a single membrane to rapidly detect nucleotide sequence variation in unamplified genomic DNA.

Fabrication methods must be re-evaluated in order to find the best technique suited for creating such large nanopore arrays. The arrays described in this section serve as a useful platform for testing scaling properties of nanopore array genotyping methods.

Initially, the TEM drilling technique described in Section 2.2 was repeated on the same membrane to create a 3 x 3 array. Figure 2.8 shows the 3 x 3 array of nanopores with the diameter of each nanopore ~ 5 nm and a pitch (spacing between adjacent nanopores) of $5 \mu\text{m}$. The total time taken to make such an array was ~ 1 hour or just under 7 minutes per nanopore. At this rate, creating 40 – 50 nanopores would take over 5 hours. Fabrication time can be significantly reduced by marking nanopore locations and by reducing the thickness of the membrane.

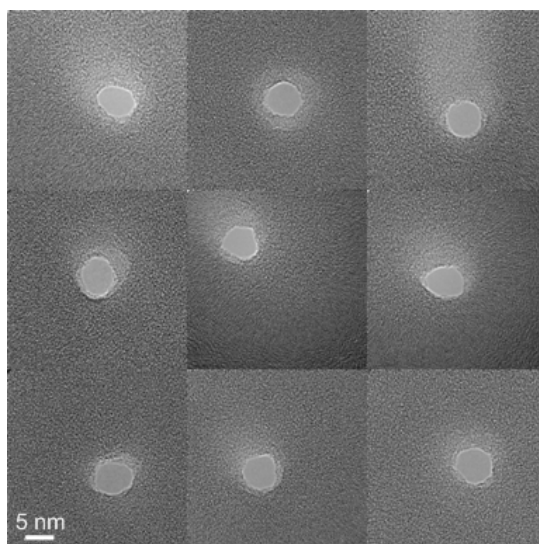


Figure 2.8: A 3 x 3 array of ~ 5 nm nanopores with a pitch of $5 \mu\text{m}$. Since the pitch is 1000 times the dimension of the nanopore, each individual nanopore picture has been stitched together to help visualize the array. Scale bar is 5 nm.

The time taken to create a nanopore is directly related to the thickness of the membrane. Thinning down the membrane prior to TEM drilling would reduce the time taken to create the array. A focused ion beam

(FIB) is widely used to mill thin sample slices to be viewed in a TEM. It is also equipped with software that enables the user to create an array of circular pits with the desired dimensions within minutes.

FEI's Dual Beam Strata 235 was available to us which uses gallium ions as the source, at a fixed energy of 30 keV. Gallium ions are heavier than electrons and therefore ablate the sample at lower energies. In order to preserve mechanical stability, only the area surrounding each nanopore was thinned. The resulting pits shown in Figure 2.9 were easily visible under the TEM and then became the sites for the creation of nanopores.

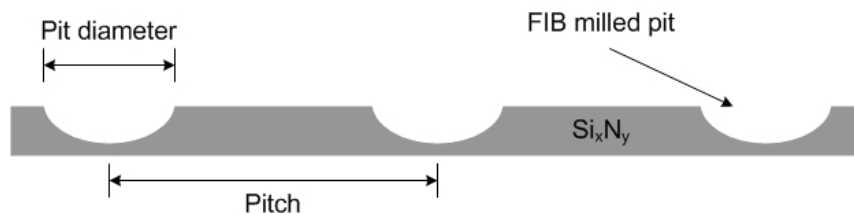


Figure 2.9: Cross-section diagram showing the FIB created pits in the SiN membrane. The pitch and the pit diameter are user controlled.

The associated FIB software enables the user to specify the feature dimensions, pitch and time of exposure to the ion beam. Arrays of circular pits, 50 nm to 300 nm in diameter, were created with a pitch of 100 nm to 500 nm, respectively. Intact arrays of pits were selected as the basis for nanopore arrays.

The TEM drill time was used to calculate the pit depth, assuming a linear relationship between membrane thickness and nanopore drilling time. Thinning the membrane reduced drilling time from 1 min to ~ 15 s per nanopore, giving an average reduction in membrane thickness of 20 nm. At just under 3 minutes per nanopore, a total of 44 pores were drilled in about two hours, with 50 nm diameter pits on a 100 nm pitch. These would have taken over five hours to drill with an un-thinned membrane. Figure 2.10 shows a 5 x 5 array from that set with further magnified pictures (Figure 2.10 (b) – (d)), the last one showing a 4 nm nanopore in the FIB pit.

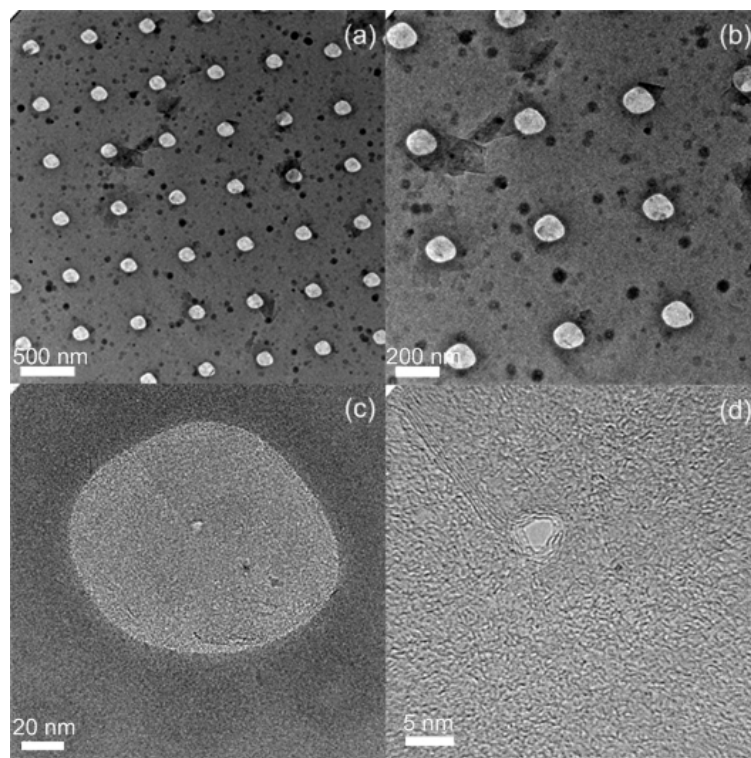


Figure 2.10: (a), (b), (c): A nanopore-in-pit array to showing a single 4 nm nanopore in (d). 44 nanopores were drilled in the TEM in two hours. Scale bars are (a) 500 nm, (b) 200 nm, (c) 20 nm and (d) 5 nm.

Challenges when creating these arrays were in the form of inaccurate ion beam alignment, which led to elliptical pits instead of circular pits and over exposed areas, which created arrays of holes instead of arrays of pits. Beam alignment for the FIB is similar to that of the TEM, although the ion beam will damage the sample during alignment. Generally, alignment is performed on an area of the sample that can be sacrificed or on a separate test sample.

As mentioned earlier, the reduced array fabricated using the TEM technique is useful to develop and test nanopore force spectroscopy using the existing experimental setup. For the development of a prototype genomic device (> 100,000 nanopores in a single membrane) however, new methods of creating larger arrays must be explored. Reducing the diameter of larger nanopores (> 10 nm) by electron beam [23, 25] and ion beam [22] exposure is a popular technique presented in literature. Creating a larger array of several thousand nanopores with diameters above 10 nm is well established by methods such as direct FIB milling or a combination of electron beam lithography and reactive ion etching. The drawbacks to such an approach lie in the time taken to create an array of over a hundred thousand nanopores and the variation seen in nanopore diameters over a single array.

One successful technique of creating several thousand 5 nm nanopores in a silicon membrane was demonstrated by Striemer et. al.

[42]. A free standing amorphous silicon membrane is annealed leaving behind a crystalline membrane with sub-10 nm nanopores. Such a speedy technique is highly compatible with large scale production and is being actively looked into for nanopore work, though at present there may be too much variability in the pore sizes of such arrays.

Simultaneously, the performance of a single synthetic nanopore must first be investigated. The required hardware and software were designed in-house and are detailed in chapter 3.

CHAPTER 3 EXPERIMENTAL SETUP

One of the advantages of nanopore based analysis is the use of a purely electrical detection technique. For typical electrolyte concentration of 1 M KCl, the resistance of a nanopore is on the order of hundreds of mega ohms resulting in currents from hundreds of picoamps to a few nanoamps under an applied voltage of a few hundred millivolts. High sensitivity measurements therefore require minimization of external noise sources.

The measurement apparatus consists of an electrochemical cell with two chambers separated by a single nanopore in a free-standing silicon nitride membrane supported by a silicon chip. The nanopore chip is the only ionic pathway between the chambers filled with a conductive, buffered electrolyte solution of 1M KCl, 10 mM HEPES at pH 7.0. Ag/AgCl electrodes² from each chamber are attached to a patch clamp amplifier that is capable of measuring up to 20 nA of current with pico-ampere sensitivity.

² The electrodes are made by soaking silver wire (Alfa Aesar, 99.9% purity) in a bleach solution for at least 30 mins.

The patch clamp amplifier is computer controlled (NI-DAQ 16 bit A/D card) with customized software (National Instruments LabVIEW platform) for real time data acquisition. The electrochemical cell is housed in a gold coated aluminium housing assembly that serves as a Faraday cage to reduce electromagnetic interference. Figure 3.1 shows a schematic of the complete arrangement. The housing assembly, nanopore cell and gaskets were all designed in-house (see Appendix B for dimensioned drawings).

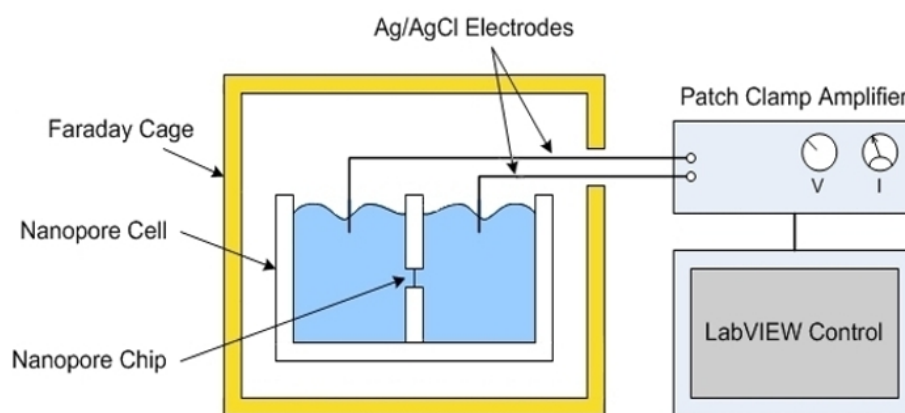


Figure 3.1: Synthetic nanopore experimental setup where the nanopore chip separates the two chambers of the electrochemical cell and the nanopore cell is housed in a Faraday cage. The electrodes are attached to a computer controlled patch clamp amplifier.

The nanopore cell sits in the housing assembly and the electrodes are clamped into position. Although there was no specific temperature control used for the work in this thesis, a base plate heating block served as the bottom of the housing assembly. Figure 3.2 shows how the entire assembly fits together along with the electrodes. Note that the cover is not shown but is designed to surround the two electrodes

and the nanopore cell. The entire setup including the nanopore cell, housing and the patch clamp amplifier head stage sits on a vibration isolation table with air suspension.

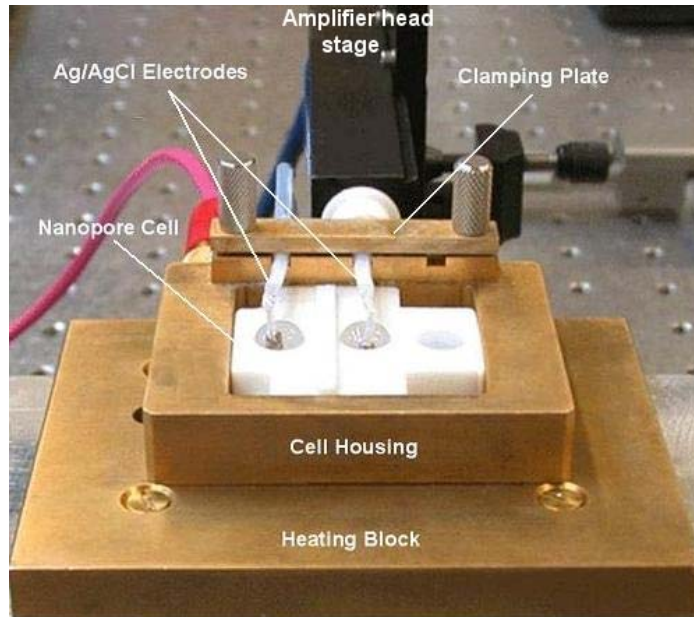


Figure 3.2: Gold coated synthetic nanopore housing assembly showing the nanopore cell with the clamped electrodes connected to the amplifier head stage. A gold coated aluminium cover (not shown here) sits over top of the electrodes against the clamping plate to complete the Faraday cage.

The noise reducing gold coating of aluminum and stainless steel parts was done as follows. Aluminum parts were first passivated with zinc after oxide etching (Zincate solution, Caswell Inc.) then replaced with 7 μm of nickel (Electroless Nickel Kit, Caswell Inc.). All parts then received 100 nm – 300 nm of gold via electroless deposition (Insta-Gold Flash Bath, Gold Touch Inc).

The nanopore cell is custom made from Poly-tetra-fluoro-ethylene (PTFE). Other materials such as poly-ether-ether-ketone (PEEK) and MACOR® (machinable glass ceramic) were also investigated. PTFE however, was the easiest material to work with due to its inert chemical properties, the relative ease of machining, availability and relatively low cost. The cell was designed to be a two piece clamped cell with the synthetic nanopore chip sandwiched in between as seen in Figure 3.3.

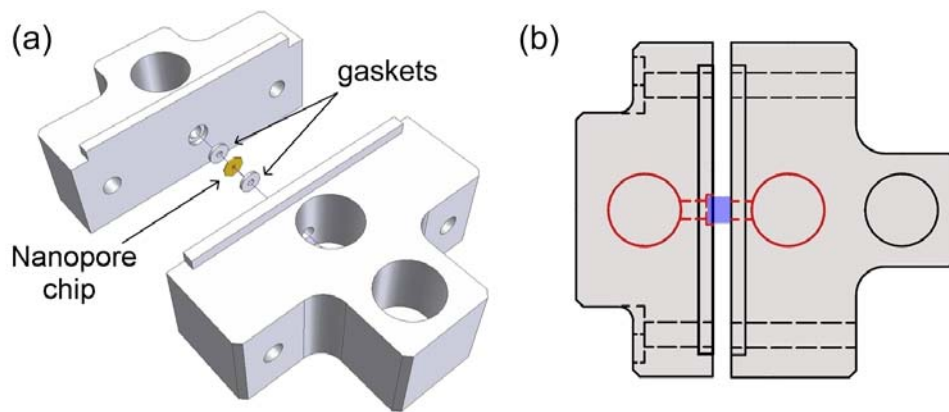


Figure 3.3: (a) Synthetic nanopore cell showing the two piece clamping assembly with the nanopore chip sandwiched in between two gaskets. (b) Top view of the assembly showing the position of the nanopore chip and gaskets (blue) between the two chambers of the electrochemical cell (red). The third chamber is engineered with future work in mind such as variable temperature experiments.

The nanopore chip (coloured blue in Figure 3.3 (b)) must be the only fluidic channel between the two reservoirs (coloured red in Figure 3.3 (b)). To seal the chip, silicone elastomer gaskets with an outer diameter of 0.08" (2.032 mm) were punched out of a 0.015" (0.381 mm) thick sheet of silicone (white silicone rubber film, McMaster-Carr

part # 86435K33) using a custom made stainless steel hole punch. The inner diameter of 0.04" (~1 mm) was made using a blunt tip needle. Punches were mounted on a non-rotating drill press to ensure even pressure while punching. A tight seal is achieved by clamping the two pairs of flanges on the cell using a stainless steel screw and nut.

The nanopore cell design (see Appendix B for dimensioned drawings) has been improved over earlier versions as follows. The clamping flanges of the cell were made thicker in order to avoid deformation due to clamping pressure and to ensure that the cell can be reused several times. Although the hydrophobic nature of PTFE helps to avoid wicking and spreading of fluid, wedges were created on the top of the cell at the clamping interface to guard against accidental splashing and cross contamination between the two reservoirs by the user. A set of milling bits are designated solely for machining nanopore cells to avoid contamination.

Proper setup of the nanopore cell is the most crucial part of the experimental setup protocol since the chip is prone to damage at this stage due to user handling. In order to achieve proper wetting of the nanopore, a low surface tension fluid such as ethanol is first introduced into the reservoirs. The cell is placed under vacuum (produced by a water based venturi pump) to remove any residual air pockets within the small channels leading to the nanopore chip. The ethanol solution is then replaced by perfusing approximately three times the total

reservoir volume of the cell with electrolyte solution. The electrodes are then submerged into the two chambers and clamped into position. The top cover is placed over the electrodes and cell to close the Faraday cage. Recording and analysing the current signal is done via computer control. The following chapters look into the characteristics of the nanopore that can be extracted from this recorded current through the nanopore.

CHAPTER 4 CHARACTERIZATION OF SYNTHETIC NANOPORES

Knowledge of the three dimensional (3D) geometry of a nanopore is useful for determining the electric field within the nanopore, and thus the force seen by the DNA strand during force spectroscopy. The region of strongest field is located at the narrowest constriction, the projection of which is seen in the TEM images. An understanding of the 3D geometry is also useful to account for any geometry dependent DNA–nanopore interactions seen during experiments.

Recently, 3D tomography has shown that a silicon nitride nanopore created using the TEM drilling technique (without further shrinking) has an ‘hour glass’ structure [24]. This confirmed earlier reports of a double cone cross-section [20]. 3D tomography required sophisticated instrumentation that was not easily accessible to the author. Here, the double cone model along with the extracted conductance value is used to estimate the dimensions of a given nanopore.

The conductance of a nanopore is dependent on its 3D geometry and can be used to estimate the cross-sectional profile for a given nanopore. The conductance, which is the inverse of resistance, is the slope of the current vs. voltage graph (IV curve) and determines the

value of the open pore current at any voltage. Conductance measurements are made in the absence of DNA. This chapter uses the IV curves to estimate the cross-sectional profile of a nanopore using the double cone model.

In our experience, most of the nanopores fabricated using the TEM technique described in Chapter 2, have linear IV curves. Current values are recorded over a voltage range of -200 mV to +200 mV. The conductance value of the nanopore is derived from fitting the IV curves to a straight line. Significant deviations from the linear trace can indicate improper wetting of the nanopore, clogging due to the presence of bubbles in the reservoir channels leading to the nanopore chip, asymmetrical geometry of the nanopore or a significant presence of surface charges near the nanopore or on its wall. Clogging or improper wetting of the nanopore show up as low conductance IV curves while leakages show up as high conductance IV curves. Figure 4.1 shows the TEM image of a ~3 nm diameter nanopore and its corresponding IV curve in a 1M KCl solution at pH 7 with conductivity of 12 S/m. The conductance of the nanopore is 9.02 nS.

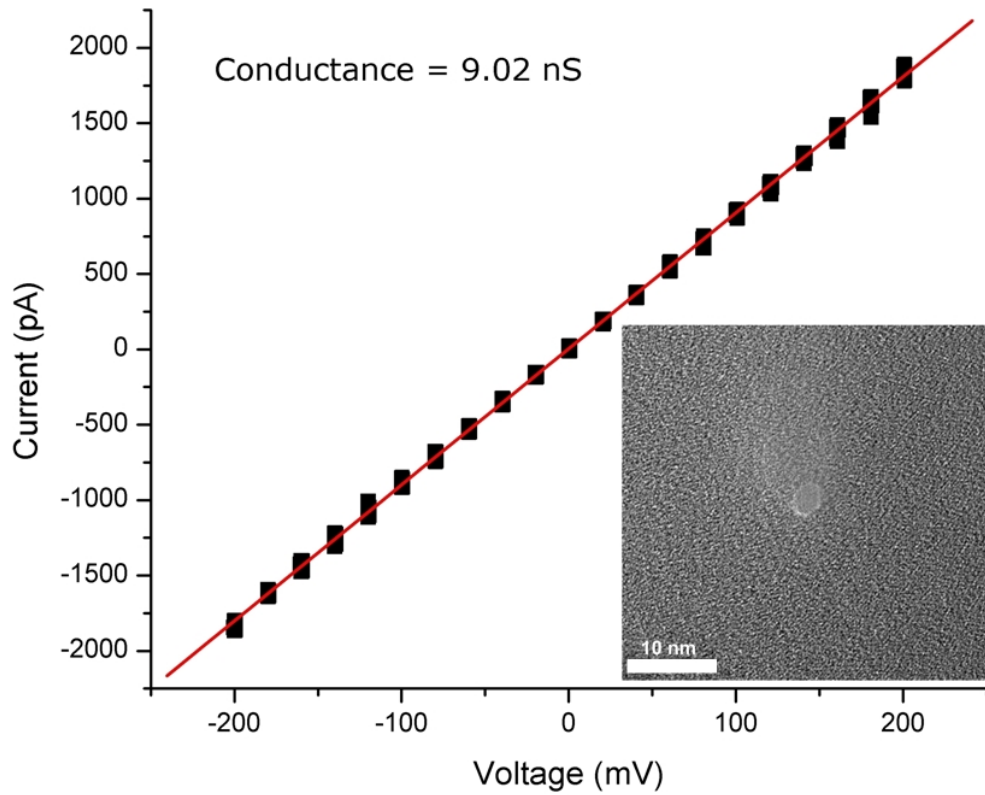


Figure 4.1: IV graph for a 3 nm nanopore (inset) over an applied voltage of -200 mV to 200 mV.

Figure 4.2, can be used to estimate the cross-sectional profile for the nanopore in Figure 4.1. The diameter of the base (d_{base}) and the half cone angle (θ) varies from nanopore to nanopore. It is important to note that not all nanopores have a perfectly symmetric double cone structure, as seen in Chapter 2, due to the presence of electron beam drift during nanopore drilling and astigmatism in the electron beam.

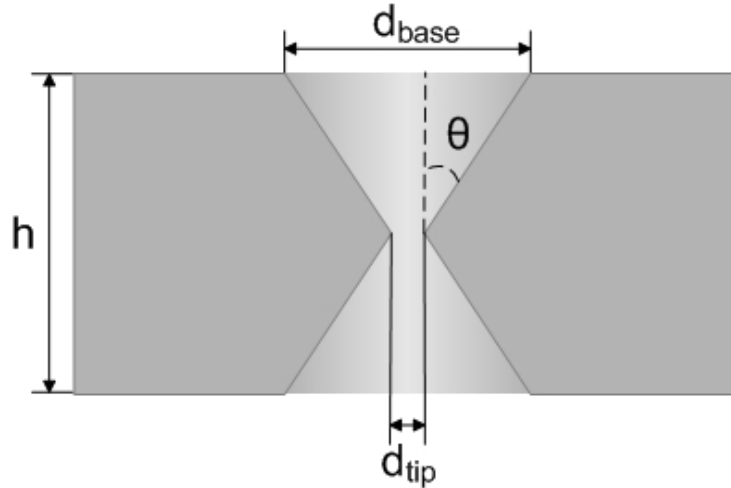


Figure 4.2: Model of double cone nanopore geometry where a TEM image would only show the narrowest diameter d_{tip} . The widest part of the nanopore d_{base} , is generally assumed to be at the surface of the membrane. The height h of the conical structure is 30 nm.

The following equation represents the resistance (R) of a cylindrical tube with varying cross-section [35],

$$R = \rho \int \frac{dz}{A(z)} \quad (4.1)$$

Where $A(z)$ is the cross-sectional area perpendicular to the length coordinate z and ρ is the resistivity. The resistance of a linearly tapering cone can then be derived by using an effective radius,

$$r_{eff} = \sqrt{r(0) * r(h)} \quad (4.3)$$

Where $r(0) = \frac{d_{tip}}{2}$ and $r(h) = \frac{d_{base}}{2}$ relating Figure 4.2 [43].

Using this approximation in Eq. (4.1) the conductance of the double cone,

$$G = \frac{\kappa \pi d_{base} d_{tip}}{4h} \quad (4.4)$$

Here, h is the thickness of the membrane at 30 nm, κ is the conductivity of the ionic solution and d_{tip} is the value seen in the TEM image. We can calculate the value of d_{base} using Eq. (4.4) and θ using basic geometrical relationships. Using the earlier nanopore example in Figure 4.1, we calculate a value of d_{base} to be ~ 9.6 nm and the value of θ to be $\sim 12.2^\circ$. The value of the base diameter correlates to the work shown in Chapter 2, where the area of illumination during nanopore drilling is ~ 10 nm. For this example, a diagram of the cross-section of the nanopore and electric field profile for the same are seen in Figure 4.3. The diagram also shows one possible configuration of the avidin anchored probe in the nanopore. Using the extracted conductance and double cone model we can estimate a 3D geometry for each nanopore prior to running experiments.

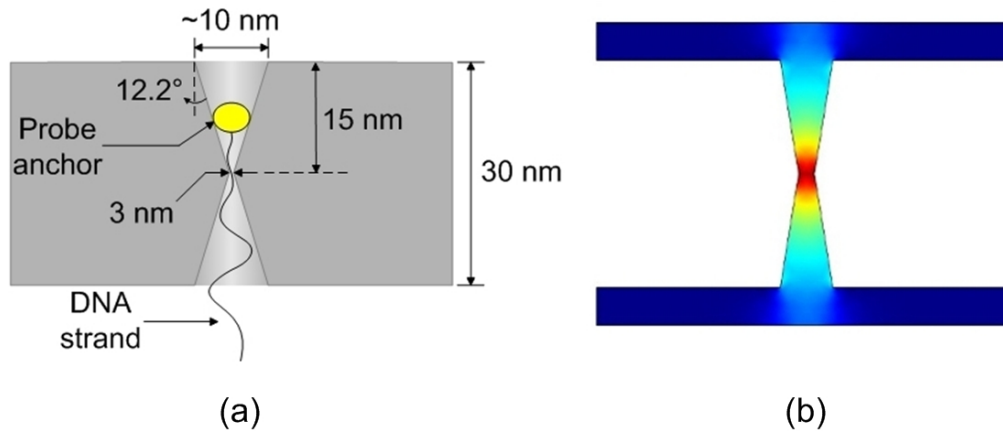


Figure 4.3: (a) Diagram showing the nanopore profile with dimensions calculated assuming a double cone model using the 2D TEM image and the measured conductance of the nanopore from Figure 4.1. The associated electric field profile for the double cone (b) structure helps visualize the force seen by a DNA strand within the nanopore. The region of highest field (red) is located at the narrowest constriction.

When recording the current vs. voltage data for each nanopore, electrical variability in the form of noise was observed. This large noise amplitude (compared to α -HL) was unexpected and was further seen in the current vs. time data. Chapter 5 discusses the known sources of noise in the experimental setup, the observation of additional noise that is related to the nanopore chip and the techniques used to reduce this noise to improve signal quality.

CHAPTER 5 NOISE ANALYSIS AND REDUCTION IN SYNTHETIC NANOPORES

A significant challenge with synthetic nanopores is the presence of electrical noise. Noise sources can include instrumentation, electromagnetic interference and the nanopore chip itself. Instrumentation noise can be minimized by feeding all computers, monitors and power supplies from the same supply circuit. Care should be taken when connecting all equipment and cables to avoid ground loops. The Axopatch 200B amplifier should be independent, to avoid noise coupling from the computer power supply. The Axopatch 200B is a patch clamp amplifier, which is designed for low noise current amplification. However, coupling between the amplifier's capacitive feedback system and the nanopore chip introduces noise into the system. Electromagnetic interference can be reduced, as seen in Chapter 3, by placing the nanopore cell in a gold-coated Faraday cage. Any excess noise seen on the current trace after taking precautions and accounting for the instrument noise was attributed to the nanopore chip itself.

Nanopore chip related noise was first observed on this system when recording the current vs. time graphs (current traces) at constant voltage as a control experiment (Figure 5.1). The noise seen on the current signal can range from 50 pA peak to peak to 200 pA peak to

peak. This compares to 1 - 2 pA root mean squared (RMS) observed in our lab in the α -HL pore, where the blockage current is 20% - 30% of its open current (~ 1 nA at 100mV). Noise in the synthetic nanopore would therefore be similar to or dominate over such current blockade values leading to undetectable events. While synthetic pores exhibit thermal and shot noise, the dominant sources are 1/f noise and dielectric noise. These are independent and can be observed on the current trace as a low frequency and a high frequency component, respectively. Figure 5.1 shows four different current traces displayed as 100 ms time segments that show the effect of noise on the open pore current at a 200 mV bias.

The dielectric noise stems from the lossy dielectric nature of the silicon nitride and the silicon chip used to fabricate the nanopore while 1/f noise is not fully understood but surface charge and conductivity fluctuations are suspected sources [44].

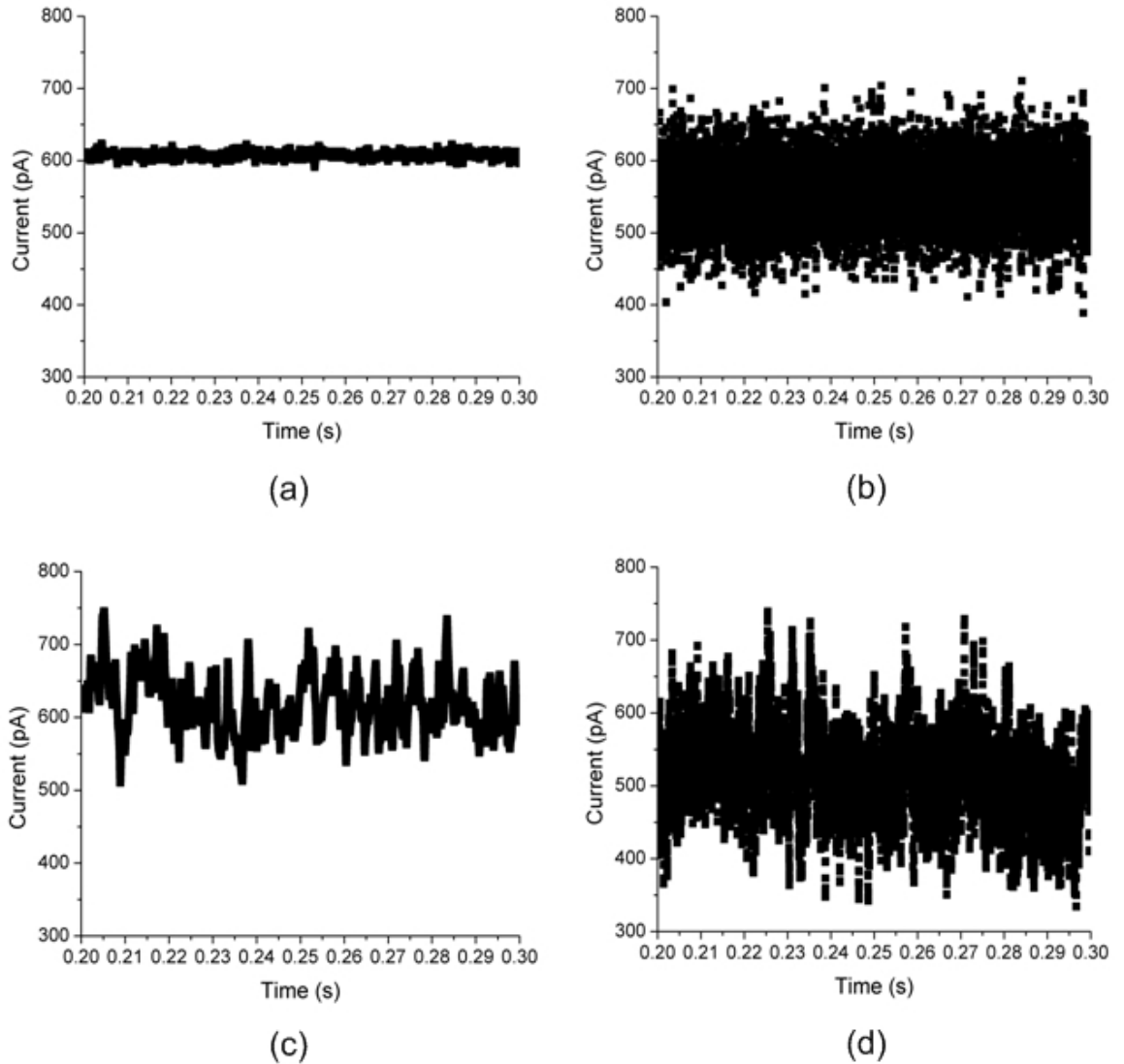


Figure 5.1: Four open pore current traces (100 ms long) at a 200 mV applied bias with low 1/f and low dielectric noise (a), with high dielectric noise (b), with high 1/f noise (c) and with both high dielectric and 1/f noise (d). The resistance of the different nanopores was 300 – 400 M Ω .

Understanding the sources of noise related to the synthetic nanopore chip provides a basis for the reduction of noise leading to improved signal quality. In this chapter, nanopore chip related noise is analyzed

using the power spectral density (PSD) and related to different material properties and dimensional constants of the nanopore chip. This chapter also looks into the techniques used to reduce the noise with associated results. The PSD measured over the bandwidth of interest, here < 20 kHz, shows thermal noise and dielectric noise at zero bias while shot noise and $1/f$ noise are seen under bias. Unless otherwise stated, all PSD measurements were recorded at a 100 kHz Bessel filter on the Axopatch 200B to avoid filter roll-off effects. The data was also split at 1600 Hz for all samples in order to increase the number of data points (minimum frequency resolution of the instrument) at low frequencies.

α -HL nanopores have very good noise properties and set a benchmark. A single α -HL nanopore in a lipid bilayer has maximum RMS current noise amplitude of 2 pA RMS while synthetic nanopores can be orders of magnitude larger. For the purpose of comparison, the PSD spectrum for α -HL was measured on the same instrument setup as that of the synthetic nanopore.

5.1 Noise Analysis at Zero Bias

The PSD (power per unit frequency) seen over a frequency spectrum can be used to distinguish between different types of noise. A SR785 signal analyzer was used to determine the PSD for different nanopores.

Different noise sources such as thermal and dielectric noise each have distinct frequency dependences, and the total noise can therefore be broken down into components by fitting the noise power spectral density to a polynomial form [45]:

$$S = a_1 + a_2 f + a_3 f^2 \quad \text{Amps}^2/\text{Hz} \quad (5.1)$$

where f is the frequency in Hertz, the a_1 term represents the thermal noise, a_2 represents the dielectric noise and a_3 describes the thermal voltage noise associated with the distributed capacitance of the $\text{Si}_x\text{N}_y/\text{Si}$ chip [45]. Similar analysis was earlier reported in patch clamping experiments that use similar instrumentation and setup. Numerical values of the coefficients are determined by fitting the measured PSD data to Eq. (5.1).

5.1.1 Thermal Noise

Thermal noise due to thermal motion of charge carriers in a resistor can be represented by Eq. (5.2) in its PSD form, as a function of the Boltzmann's constant (k), absolute temperature (T) and its resistance (R), while the root mean squared (RMS) current noise is represented by Eq. (5.3) over a specified bandwidth (B) [45, 46].

$$S_{th} = \frac{4kT}{R} \quad (\text{Amp}^2/\text{Hz}) \quad (5.2)$$

$$I_{th_{rms}} = \sqrt{\frac{4kTB}{R}} \quad (\text{Amp RMS}) \quad (5.3)$$

The RMS current noise calculated for resistors of 40 MΩ, 100 MΩ and 1 GΩ at room temperature over a 20 kHz bandwidth, is approximately 2.7 pA RMS, 1.7 pA RMS and 0.6 pA RMS, respectively. These are small values compared to the noise seen on the current signal. Since there is no frequency dependence, thermal noise is represented by a horizontal line on the PSD graph indicating the lowest noise limit achievable.

5.1.2 Dielectric Noise

Dielectric noise is related to the dielectric properties of the material. The power spectral density and the RMS current noise relationship are described below [45].

$$S_d = 4kTDC(2\pi f) \quad (\text{Amp}^2/\text{Hz}) \quad (5.4)$$

$$I_{D_{rms}} = \sqrt{4kTDC\pi B^2} \quad (\text{Amp RMS}) \quad (5.5)$$

Where (C) is the capacitance, (D) is the dissipation factor and (f) is the frequency. The capacitance of the nanopore chip is related to the dielectric constant of each layer, the area of exposure to the ionic fluid and the thickness of the individual dielectrics. The dissipation factor, also known as the loss tangent defines how much energy is lost to the environment by the dielectric material, generally in the form of heat.

Mathematically, it is the ratio of the imaginary to the real coefficients of permittivity (Eq. 5.6) [45, 46].

$$D = \frac{\mathcal{E}_{imaginary}}{\mathcal{E}_{real}} \quad (5.6)$$

The dissipation factor is a function of frequency and temperature; however, between 1 kHz – 100 kHz at room temperature, it is assumed to be a constant [22]. Eq. (5.4) shows that the PSD is proportional to the product of the dissipation factor and the capacitance. In this case, the large noise implies a large DC product due to a relatively large area of exposure, dielectric constant and dissipation factor.

The third term a_3 rises as f^2 and is comprised of thermal voltage noise coupled to the distributed capacitance of the ionic fluid to $\text{Si}_x\text{N}_y/\text{Si}$ chip interface. By fitting Eq. (5.1) to the PSD data, as seen in Figure 5.2, numerical values of the three coefficients are extracted for a nanopore chip and α -HL and Table 5.1 lists these values. The coefficient a_2 representing the dielectric noise, is two orders of magnitude higher for a Si_xN_y nanopore than that for α -HL.

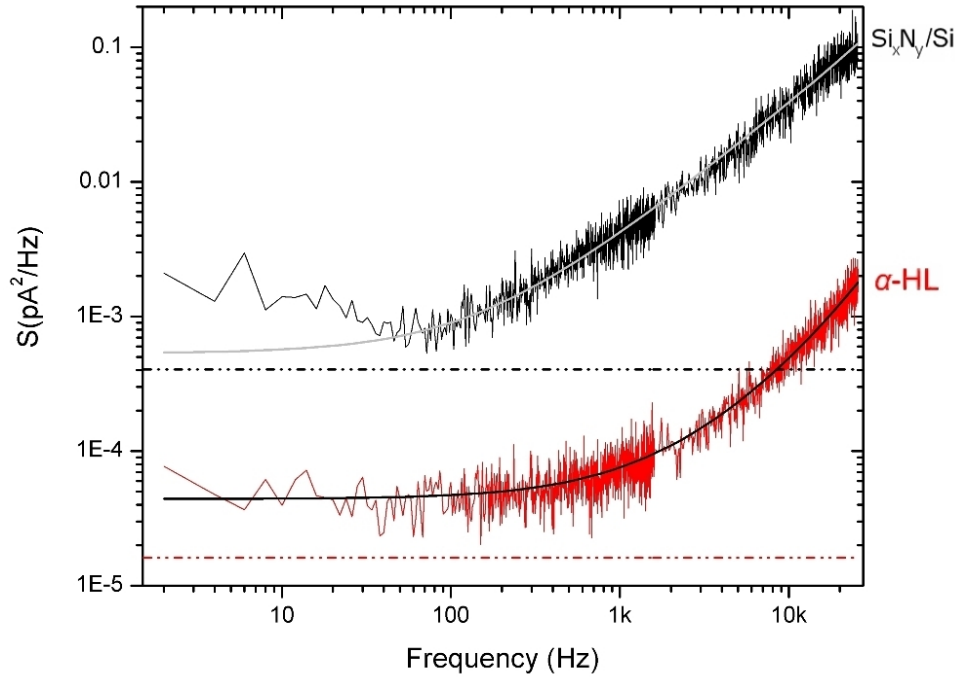


Figure 5.2: The PSD of a $\text{Si}_x\text{N}_y/\text{Si}$ chip and that of $\alpha\text{-HL}$ is fitted to Eq. (5.1) to determine the three coefficients. The hashed lines are the thermal noise given the resistance ($\sim 40 \text{ M}\Omega$, $\sim 1 \text{ G}\Omega$) of the nanopores at room temperature.

Table 5.1: Numerical values determined from fitting the PSD to Eq. (5.1). The large difference in terms a_2 and a_3 arise due to the difference in dielectric properties of the $\text{Si}_x\text{N}_y/\text{Si}$ chip and $\alpha\text{-HL}$.

	a_1	a_2	a_3
$\text{Si}_x\text{N}_y/\text{Si}$	$5.3 (\pm 3.4) \times 10^{-4}$	$3.68 (\pm 0.03) \times 10^{-6}$	$1.8 (\pm 0.1) \times 10^{-11}$
$\alpha\text{-HL}$	$0.4 (\pm 0.062) \times 10^{-4}$	$0.03 (\pm 0.002) \times 10^{-6}$	$0.15 (\pm 0.008) \times 10^{-11}$

The dielectric noise seen on the signal at zero bias is dependent on the capacitance, which is in turn dependent on the area and inversely to the thickness of Si_xN_y membrane exposed to the ionic fluid. Covering this area will decrease the capacitance of the chip reducing the overall noise. Section 5.3 discusses this technique further.

5.2 Noise Analysis under Bias

Once a bias voltage is applied across the nanopore, voltage dependent noise is seen in addition to the noise at zero bias. $1/f$ noise is the dominant noise source at low frequency as seen in Figure 5.3, where the PSD for a single nanopore at 0 mV and 200 mV is plotted over a 20 kHz bandwidth. The presence of ionic current also gives rise to shot noise, and both noise components are further discussed in the following sub-sections.

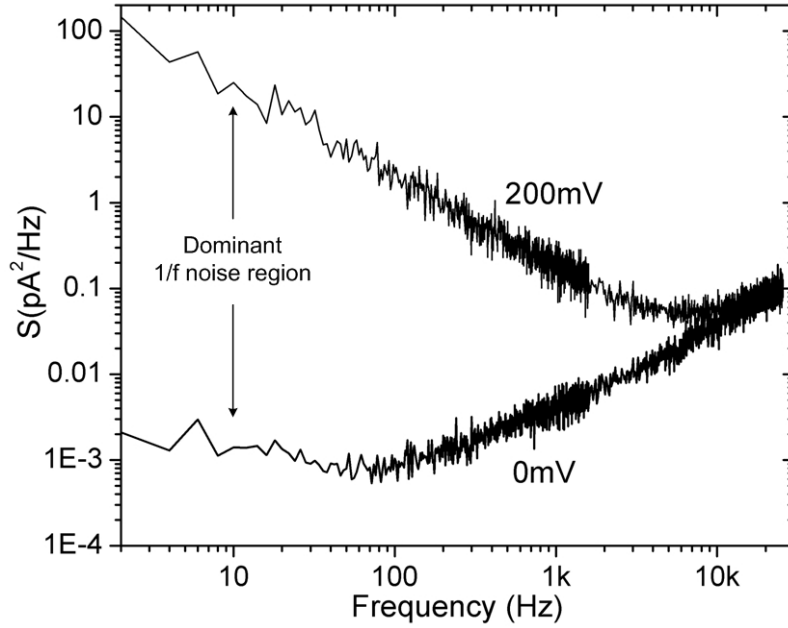


Figure 5.3: The PSD of a $\text{Si}_x\text{N}_y/\text{Si}$ chip at zero bias and at 200 mV. The 1/f noise is dominant at low frequency.

5.2.1 Shot Noise

Current is determined by the movement of ions across the nanopore. Statistically, the number of ions that move across the nanopore at any time varies, resulting in generation of shot noise. The PSD and the RMS current noise due to shot noise can be represented as a function of the basic unit charge (q), the DC current (I) in Amps and the bandwidth (B) [22].

$$S_s = 2qI \quad (\text{Amp}^2/\text{Hz}) \quad (5.7)$$

$$I_{s_{rms}} = \sqrt{2qIB} \quad (\text{Amp RMS}) \quad (5.8)$$

The RMS current noise calculated for resistors of 40 M Ω , 100 M Ω and 1 G Ω under a 200 mV applied voltage, at room temperature, over a 20 kHz bandwidth, is approximately 5.6 pA RMS, 3.6 pA RMS and 1.1 pA RMS, respectively. Similar to thermal noise, there is no frequency dependence here and hence shot noise is represented by a horizontal line on the PSD graph. Shot noise added to thermal noise gives the lowest noise limit achievable under bias.

5.2.2 1/f Noise

1/f noise has been observed in semiconductor devices [44, 47], carbon nano-tubes [48] and synthetic membranes [49-51]. Although 1/f noise is not well understood, there is general agreement that it stems from conductivity fluctuations. Conductivity is directly proportional to the number of charge carriers and their mobility, leading to two separate models that describe these fluctuations. The mobility fluctuation model described by Hooge explains 1/f noise as a bulk phenomenon arising from the fluctuating mobility of the charge carriers [44]. The number fluctuation model described by McWhorter, explains 1/f noise as a surface phenomenon arising from the fluctuating number of charge carriers [47].

The presence of contaminants on the surface of the Si_xN_y leads to inhomogeneous surface charge effects that can contribute to the reduction of the number of charge carriers within the nanopore. Further to this, Dekker et. al. also see that the presence of nano

bubbles in the nanopore create $1/f$ noise characteristics [51]. The variation of the bubble size due to thermal fluctuations inside the pore modulates the conductance and generates this $1/f$ noise. These bubbles originate due to the hydrophobic nature of the surface and possibly from the gas present in the ionic solutions. Therefore, surface phenomena are perceived to be the main contributor of $1/f$ noise in this system.

Degassing solutions used during experiments and cleaning the surface of the nanopore has shown great improvement in the reduction of $1/f$ noise (section 5.3). The following section looks into the techniques used to reduce both dielectric and $1/f$ noise.

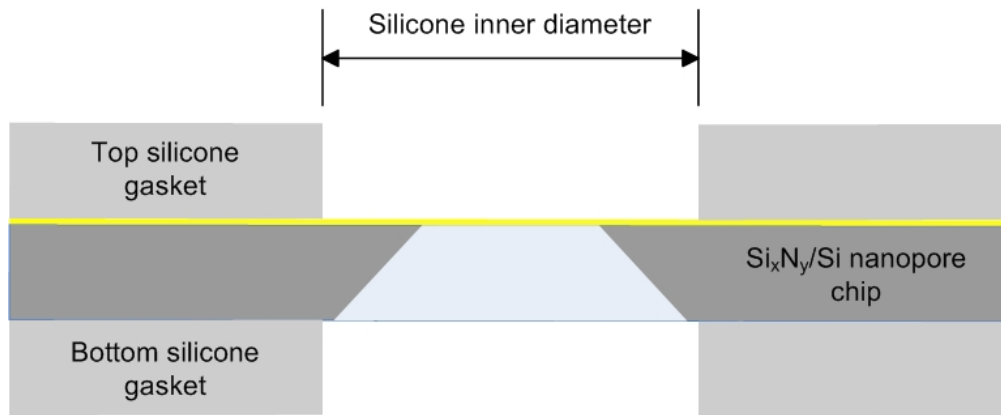
5.3 Methods to Reduce Noise

Dielectric noise and $1/f$ noise stem from independent noise sources and therefore can be reduced individually. As seen in the previous sections, the high dielectric noise is a result of the large capacitance of the $\text{Si}_x\text{N}_y/\text{Si}$ chip while inhomogeneous surface charge and contaminants are the suspected cause of $1/f$ noise. Addressing these specific sources and developing reduction techniques improves the performance of the nanopores further enabling their use in a genotyping device. The following sub-sections detail these techniques and compare the PSD for a nanopore that underwent noise reduction

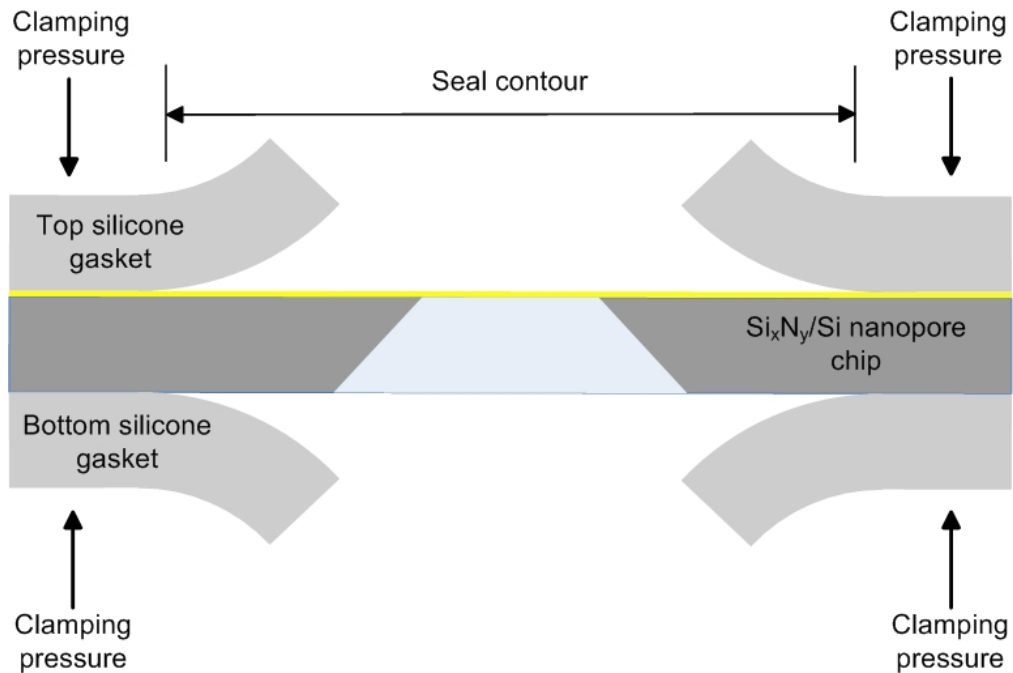
techniques. Note that the PSD for this nanopore was also taken on the same experimental setup as that for the untreated nanopore and α -HL.

5.3.1 Reduction of Dielectric Noise

The capacitance of the $\text{Si}_x\text{N}_y/\text{Si}$ chip is proportional to the area of the ionic solution in contact with the chip. For qualitative purposes we assumed that the area defined by the inner diameter of the silicone gasket (~1 mm as seen in Chapter 3) was the area of the capacitive plate; however, as seen in Figure 5.4, this area is larger. The silicone gaskets are placed on either side of the chip to ensure proper sealing. The two sides of the cell exert pressure on the gaskets, creating a seal contour which is the same as the circumference of the PTFE bore connecting the fluid reservoirs to the chip. There is poor gasket-to-chip adhesion where no clamping pressure is present and the buffer solution seeps under the exposed gaskets up to the seal contour (Figure 5.4 (b)), increasing the area of the capacitive plates and hence the capacitance.



(a)



(b)

Figure 5.4: Cross-section diagram of the two silicone gaskets and the nanopore chip assembly. When there is no clamping pressure on the assembly (a), the silicone gaskets sit comfortably on the nanopore chip. Once the assembly is subjected to a clamping force (b), the poor adhesion of the gaskets results in the electrolyte seeping under the gaskets up to the seal contour created by the PTFE cell.

Reducing the area of exposed thin Si_xN_y membrane to the ionic solution reduces the nanopore chip capacitance. In patch clamping experiments, poly-di-methyl-siloxane or PDMS (Dow Corning Sylgard 184) is used to cover the tip of the pipette to reduce dielectric noise in that system; hence, a similar technique is applied here, where the relatively thick PDMS layer is painted over the Si_xN_y layer ($10\ \mu\text{m}$ vs. $30\ \text{nm}$) up to the free standing membrane window to reduce the Si_xN_y area exposed to the ionic solution. In addition to this, the dielectric constant and dissipation factor of PDMS is lower compared to both Si_xN_y and Si thereby lowering the dielectric noise further [52]. Note that PDMS adheres more strongly to a Si_xN_y layer that has undergone an organic cleaning step such as piranha cleaning prior to PDMS painting.

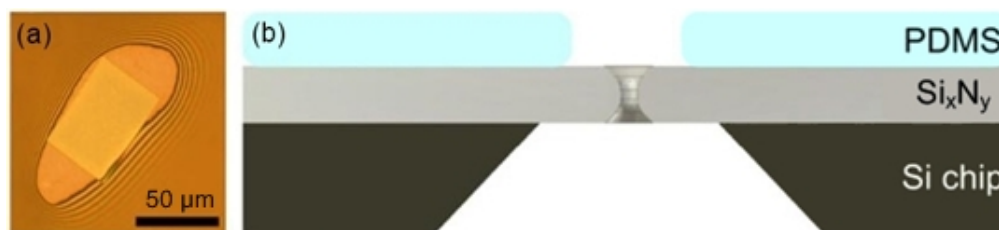


Figure 5.5: (a) Optical top view image of a PDMS coated nanopore chip showing the PDMS close to the freestanding membrane window (b) Cross-section of PDMS painted nanopore chip (not to scale)

Painting PDMS on the silicon nitride surface is done manually, by carefully thinning out a drop of PDMS mixture over the Si_xN_y layer using a single loop paint brush. Figure 5.5 (a) shows the optical image of a nanopore chip with a layer of PDMS over top, while a diagram of

the cross-section is seen in Figure 5.5 (b). The thickness of the PDMS layer is $\sim 10 \mu\text{m}$, as measured using an alpha step stylus profilometer. Once the PDMS is painted, it is left for 20 minutes in a $100 \text{ }^\circ\text{C}$ oven to dry. This nanopore chip is now ready to be used in the nanopore setup as described in Chapter 3.

Nanopore chips with PDMS painted on them showed a reduction in the dielectric noise by at least an order of magnitude. The noise trace (Figure 5.6 (a)) and the PSD (Figure 5.6 (b)) for a bare $\text{Si}_x\text{N}_y/\text{Si}$ chip, a PDMS painted nanopore chip and $\alpha\text{-HL}$ are shown at 0 mV.

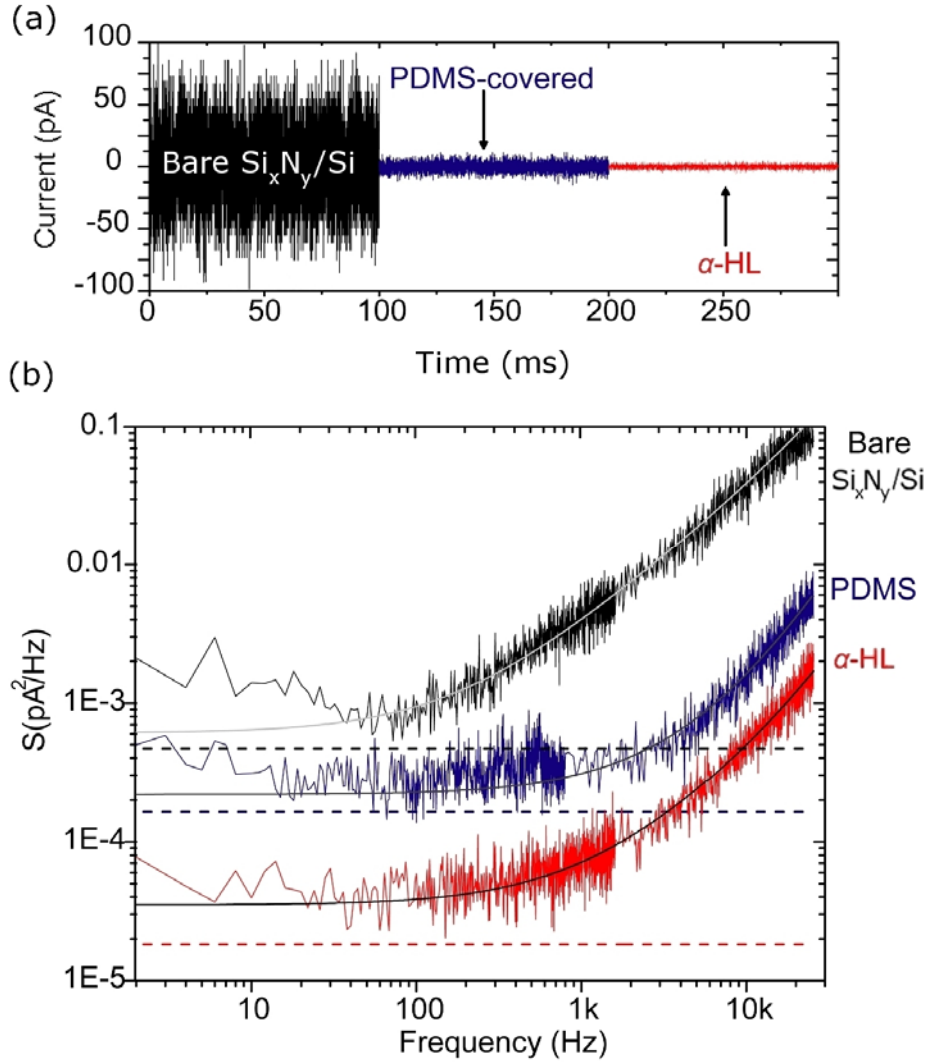


Figure 5.6: (a) Current vs. time (sampled at 100 kHz with a 10 kHz low pass Bessel filter) traces at zero bias for a bare Si_xN_y/Si nanopore chip (black), PDMS coated chip (blue) and that of α -HL (red). (b) PSD showing the effect of PDMS on the noise spectrum (here the PDMS data is split at 800 Hz). All three data sets are fit to Eq. (5.1) and their numerical values are tabulated in Table 5.2. The dashed lines are the thermal noise limit for the three nanopores with resistance of $\sim 40 \text{ M}\Omega$, $\sim 100 \text{ M}\Omega$ and $\sim 1 \text{ G}\Omega$ for bare Si_xN_y/Si, PDMS coated and α -HL, respectively.

Fitting all three PSD curves to Eq. (5.1), we see that coefficients a_2 and a_3 are in the same order of magnitude for both α -HL and the PDMS coated chip due to the reduction of dielectric noise. **Error! Reference source not found.** shows the values of the three coefficients for each curve.

Table 5.2: Numerical values determined by fitting the PSD data sets using Eq. (5.1).

	a_1	a_2	a_3
Bare Si _x N _y /Si	$5.3 (\pm 3.4) \times 10^{-4}$	$3.68 (\pm 0.03) \times 10^{-6}$	$1.8 (\pm 0.1) \times 10^{-11}$
PDMS	$3.1 (\pm 0.2) \times 10^{-4}$	$0.07 (\pm 0.006) \times 10^{-6}$	$0.61 (\pm 0.03) \times 10^{-11}$
α -HL	$0.4 (\pm 0.062) \times 10^{-4}$	$0.03 (\pm 0.002) \times 10^{-6}$	$0.15 (\pm 0.008) \times 10^{-11}$

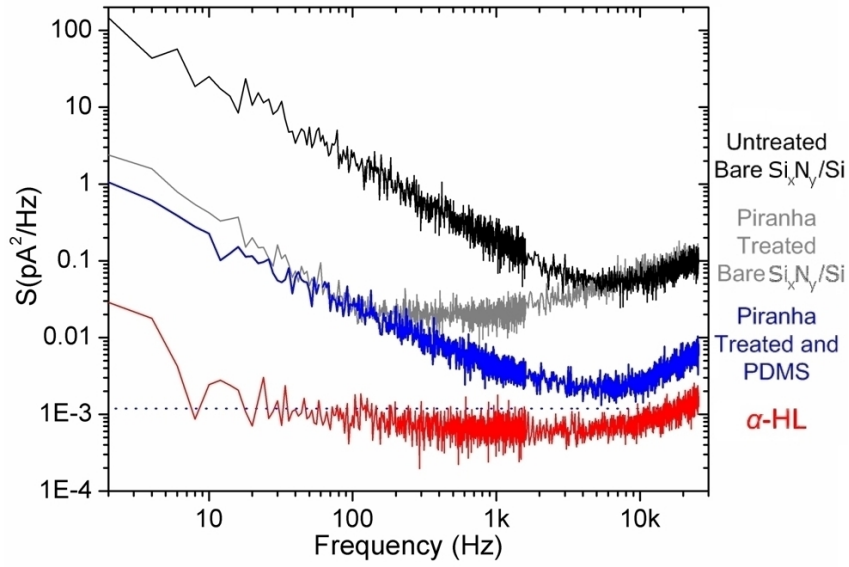
Reducing the capacitance of the membrane gives better noise characteristics, increasing the reproducibility of our experimental data and increasing the signal-to-noise ratio (SNR) to a level at which we can easily identify and analyze current blockade events.

5.3.2 Reduction of 1/f Noise

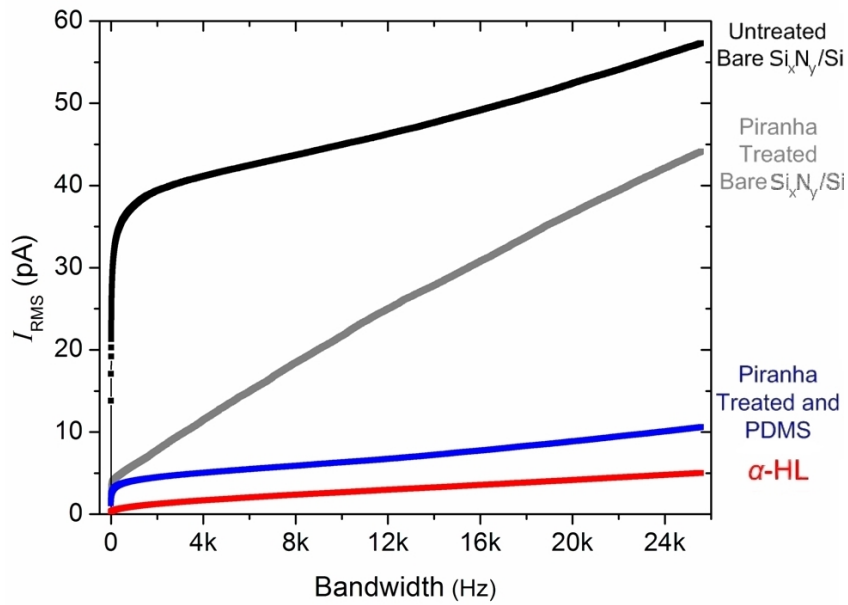
1/f noise is likely due to static or dynamic surface charges or contaminants on the Si_xN_y surface and the presence of small air bubbles in the ionic solution. Freeing the surface of unwanted charged species and removing air bubbles from all solutions used during

experiments is a good noise reduction technique. One of the more common chemical cleaning agents is piranha (H_2SO_4 : H_2O_2 : : 3:1), which removes all organics from the surface. This makes the surface hydrophilic making for easier wetting of the nanopore. It also lowers the probability that any surface edges will harbour small air pockets leading to nano bubble formation [51]. Degassing all solutions that are used in experiments by ultrasonication and mild heating for 10 minutes followed by vacuum pumping on the solution, reduces the number of air bubbles in the solution and helps reduce $1/f$ noise. Nanopores used for experiments are subjected to this rigorous noise reduction protocol of piranha cleaning and PDMS painting as it results in good signal quality.

Three different nanopores were used for protocol comparison and the corresponding PSD data plotted against that of α -HL seen in Figure 5.7 (a). The PSD for all four nanopores is taken at an applied voltage of 200 mV. The untreated nanopore shows the maximum noise (black data set). A nanopore that is only treated to a $1/f$ noise reduction technique (grey data set) shows a drop in magnitude in the low frequency noise spectrum, while a nanopore treated to both the $1/f$ and the dielectric noise reduction techniques shows a drop in magnitude across the entire noise spectrum (blue data set). Figure 5.7 (b) shows the effect of each noise reduction technique to the RMS current for all four nanopores.



(a)



(b)

Figure 5.7: (a) PSD for an untreated nanopore (black), a nanopore subjected to only 1/f noise reduction (grey), a nanopore subjected to both 1/f and dielectric noise reduction (blue) and α -HL (red) at 200 mV applied voltage. Blue dotted line represents the shot noise and thermal noise limit for the full noise reduction treated nanopore (b) RMS current noise for the same nanopore data sets.

Assembled low noise nanopores are stored in their PTFE cells and covered by a glass Petri dish with the reservoirs filled with electrolyte. To limit the evaporation of the solution in the reservoirs, the third reservoir is filled with deionized water (DI) water and the Petri dish is wrapped in Para film. The performance of nanopores is not significantly altered after being stored in this manner for several months.

Dielectric noise due to nanopore chip capacitance and $1/f$ noise due to surface contamination are the largest contributors of noise in TEM drilled silicon nitride nanopores. Reduction in noise by up to two orders of magnitude is achieved by painting PDMS on the Si_xN_y layer (excluding the membrane window) and by piranha cleaning the nanopore surface. Nanopores subjected to both noise reduction techniques show noise characteristics that are comparable to α -HL further motivating their use for DNA detection and force spectroscopy. In order to truly compare the improvement in signal quality, low noise synthetic nanopores were used to perform DNA translocation and DNA probe capture experiments. Chapter 6 details these experiments and reports exceptional SNR values for the same.

CHAPTER 6 SYNTHETIC NANOPORE PERFORMANCE USING DNA

The performance and sensitivity of the nanopores subjected to the noise reduction techniques described in Chapter 5 were evaluated by carrying out DNA translocation and probe capture experiments.

Lambda-phage DNA (λ -DNA, 48.5 kbp double stranded DNA) was used to demonstrate translocation in these nanopores. Exceptional signal-to-noise ratios (SNR) observed during these experiments made it possible to implement force spectroscopy methods. Probe capture experiments, a precursor to force spectroscopy, involve first capturing a ssDNA probe (with an avidin-anchor) in the nanopore and then allowing the probe to thermally escape at low voltages.

When DNA passes through a nanopore, there is a decrease in conductance (current blockade) proportional to the cross-sectional area of the DNA (see Eq. 2.2). For an untreated nanopore, these values would have been difficult to obtain, due to the fluctuating nature of the open pore current (due to $1/f$ noise) and the discrepancy in the current blockade value (due to dielectric noise). Figure 6.1 shows current vs. time traces for λ -DNA translocating through a nanopore with a 6 nm diameter. The open pore current was 2.83 nA and the smallest current drop upon introduction of DNA was ~540 pA at a bias voltage of 150 mV. Using Eq. (2.2), a current blockade of ~540 pA

corresponds to a particle with a cross-sectional diameter of ~ 2 nm which is the hydrodynamic diameter of double stranded DNA (dsDNA). As seen in Figure 6.1 (a) several different current blockade levels were observed.

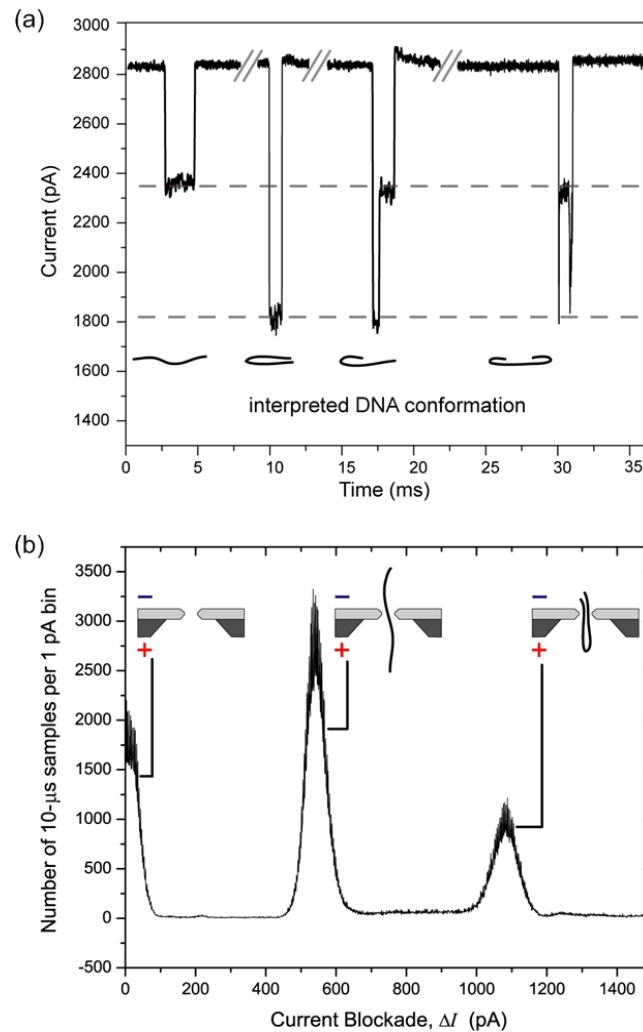


Figure 6.1: (a) Current blockade events for lambda-DNA at 150 mV bias. Current is filtered at 10 kHz and sampled at 100 kHz. The inset shows the possible configurations that the DNA takes during translocation. (b) Histogram of the current level sampled in a 10 μ s time window revealing the quantized current blockade levels representing the translocation of dsDNA through the nanopore.

The magnitude of the current blockade falls in one of the three quantized levels (Figure 6.1 (b)), implying that the DNA translocated through the nanopore in a few different configurations as seen in the inset in Figure 6.1 (a). There were three quantized states with respect to the current blockade value representing no translocation of DNA (0 pA) the translocation of a single strand of lambda-DNA ($1 \times \Delta I = 540$ pA) and a folded strand of DNA ($2 \times \Delta I = 1080$ pA) passing through the nanopore. dsDNA with a hydrodynamic diameter of ~ 2 nm can pass through a 6 nm nanopore as a single strand and as a folded strand of ~ 5 nm. Defining the SNR as the current blockade over the current RMS noise gives a value of ~ 150 for this specific nanopore chip. Note that for an untreated nanopore this value was close to 2.

Successful translocation events paved the way for probe capture experiments using a 94 nucleotide biotinylated probe anchored to avidin. Avidin is ~ 5 nm in diameter and will stop the complete translocation of DNA through a nanopore with a diameter smaller than 5 nm. Therefore, experiments using this ssDNA probe were done on a nanopore with a diameter of ~ 3 nm at a bias voltage of 300 mV. Figure 6.2 shows the capture of such a probe under bias and an eventual thermal escape at 200 mV.

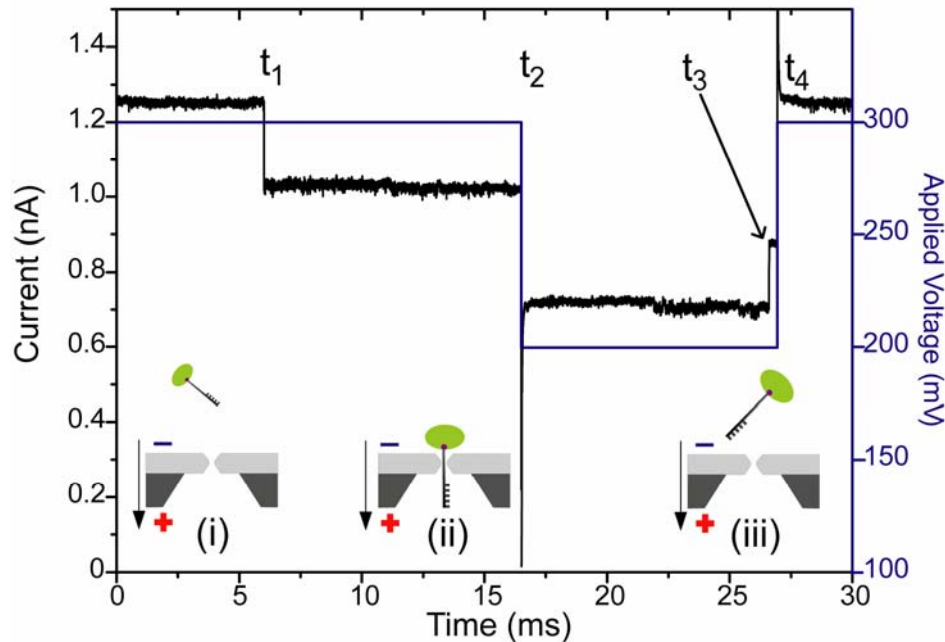


Figure 6.2: Single probe capture and escape event showing the corresponding ionic current flow (black trace) through the nanopore at a given voltage (blue solid line) and in the presence or absence of the probe molecule. The inset shows (i) the open state (ii) the probe captured state and (iii) the probe escaped open state.

At time t_1 , the probe enters the nanopore due to the initial capture voltage (here 300 mV) creating a current blockade of ~ 250 pA, which corresponds to the 1.5 nm hydrodynamic diameter of ssDNA [22]. Extensive experiments on the α -HL system have revealed that the avidin-anchor was not responsible for the observed blockade levels and that probe escape dynamics are due to DNA-nanopore interactions [22]. At time t_2 , this capture voltage is lowered (here 200 mV) with a proportional drop in the ionic current. The probe takes a finite amount of time ($t_3 - t_2$) to thermally escape over the electrostatic energy barrier. Once probe escape is observed, the system is reset (t_4)

to its initial capture voltage. For this particular nanopore, the SNR value was ~ 40 .

Noise reduction and improved fabrication of nanopores described in this thesis has improved the performance of synthetic nanopores, enabling accurate detection of single-molecule blockages. The low noise nanopores can not only detect the translocation of DNA but can be used to perform force spectroscopy experiments with unprecedented SNR values. SNR values of 40 – 150 are the best values seen to date within the synthetic nanopore community and pave the way for successful genotyping applications.

CHAPTER 7 CONCLUSION

Synthetic nanopores are being developed for incorporation into rapid clinical DNA analysis devices due to their superior durability, the precision control over the nanopore size and their compatibility with current semiconductor and microfabrication technology compared to organic α -HL nanopores. This thesis demonstrated the fabrication of nanopores on a silicon nitride membrane along with the analysis and reduction of their electrical noise characteristics

Prior to the work presented here, TEM drilled nanopores showed poor electrical characteristics threatening the development of a commercial genotyping device. Following development of improved fabrication methods we performed a careful noise analysis of the nanopore. Two distinct noise components were identified: a high frequency dielectric noise and a low frequency $1/f$ noise. The large capacitance and dissipation factor of the silicon nitride-silicon chip was identified as the source of dielectric noise and the distribution of charged species over a hydrophobic surface produced $1/f$ noise behaviour under applied voltage. Dielectric noise was greatly decreased by selectively coating the silicon nitride membrane with PDMS while $1/f$ noise was reduced by chemically removing all organics from the surface and the interior of the nanopore. In addition to this, all solutions used during experiments were degassed to minimize the introduction of gas bubbles into the

system. The resulting RMS current noise was lowered by an order of magnitude resulting in considerably enhanced nanopore performance. The low noise synthetic nanopores produced with the methods described in this thesis now show unprecedented signal-to-noise ratios from 40 to 150, enabling their use in DNA translocation and probe capture experiments. Using these pores, we were the first to implement nanopore force spectroscopy in synthetic pores, though that demonstration is not described in this thesis.

Following the success of single nanopores we pursued the development of an array of nanopores in a single membrane required for practical genotyping devices. Due to the reliability of the TEM drilling technique, an array of 44 sub-5 nm nanopores was fabricated as a proof-of-concept. Although suitable for producing small numbers of nanopores in an academic environment, producing several thousand sub-5 nm nanopores on the same membrane requires exploring alternate methods due to cost and time considerations. In addition to this, the understanding gained from the noise analysis in Chapter 5 can be used to explore different membrane materials that naturally offer lower noise contributions and therefore, different fabrication possibilities. The sub-5 nm size restriction imposed on nanopores is a fabrication challenge when creating a large array of nanopores. However, by investigating chemical passivation and synthetic deposition techniques, this size constraint can be relaxed putting it within reach of commercial semiconductor fabrication techniques. Such

techniques may offer a wider range of membrane materials while still maintaining electrical insulation and low noise characteristics.

In summary, the methods presented in this thesis have enabled the creation of nanopores whose electrical properties are defining the state-of-the-art in this field of application. The first demonstration of force spectroscopy in synthetic nanopores has since been achieved by this research group, and was enabled by the methods described in this thesis. This has generated interest in the nanopore community, which has led to new partnerships and collaborations with groups eager to use nanopores produced with the methods described here.

Consequently, this work will almost certainly play a significant role over time in the translation of nanopore methods for nucleic acid analysis to improvement of clinical molecular diagnostics.

BIBLIOGRAPHY

- [1] C. Whibley, P. D. P. Pharoah, and M. Hollstein, "p53 polymorphisms: cancer implications," *Nat Rev Cancer*, vol. 9, pp. 95-107, 2009.
- [2] B. Ferwerda, M. B. McCall, K. Verheijen, B. J. Kullberg, A. J. van der Ven, J. W. Van der Meer, and M. G. Netea, "Functional consequences of toll-like receptor 4 polymorphisms," *Molecular Medicine*, vol. 14, pp. 346-352, 2008.
- [3] A. E. Guttmacher and F. S. Collins, "Genomic Medicine -- A Primer," *N Engl J Med*, vol. 347, pp. 1512-1520, 2002.
- [4] B. S. Shastri, "SNPs in disease gene mapping, medicinal drug development and evolution," *J Hum Genet*, vol. 52, pp. 871-880, 2007.
- [5] M. Ingelman-Sundberg, M. Oscarson, and R. A. McLellan, "Polymorphic human cytochrome P450 enzymes: an opportunity for individualized drug treatment," *Trends in Pharmacological Sciences*, vol. 20, pp. 342-349, 1999.
- [6] J. S. Ross and J. A. Fletcher, "The HER-2/neu Oncogene in Breast Cancer: Prognostic Factor, Predictive Factor, and Target for Therapy," *Stem Cells*, vol. 16, pp. 413-428, 1998.
- [7] D. J. Slamon, G. M. Clark, S. G. Wong, W. J. Levin, A. Ullrich, and W. L. McGuire, "Human Breast Cancer: Correlation of Relapse and Survival with Amplification of the HER-2/neu Oncogene," *Science*, vol. 235, pp. 177-182, 1987.
- [8] S. B. Smith, Y. Cui, and C. Bustamante, "Overstretching B-DNA: The Elastic Response of Individual Double-Stranded and Single-Stranded DNA Molecules," *Science*, vol. 271, pp. 795-799, 1996.
- [9] G. D. K. Weil P. A., *Chapter 34. Nucleic Acid Structure & Function*, 27th Edition ed.
- [10] L. Z. Song, M. R. Hobaugh, C. Shustak, S. Cheley, H. Bayley, and J. E. Gouaux, "Structure of staphylococcal alpha-hemolysin, a heptameric transmembrane pore," *Science*, vol. 274, pp. 1859-1866, 1996.
- [11] L. Pugliese, A. Coda, M. Malcovati, and M. Bolognesi, "Three-dimensional Structure of the Tetragonal Crystal Form of Egg-white Avidin in its functional Complex with Biotin at 2.7 Å Resolution," *Journal of Molecular Biology*, vol. 231, pp. 698-710, 1993.

- [12] J. Nakane, M. Wiggin, and A. Marziali, "A Nanosensor for Transmembrane Capture and Identification of Single Nucleic Acid Molecules," *Biophysical Journal*, vol. 87, pp. 615-621, 2004.
- [13] C. Tropini and A. Marziali, "Multi-Nanopore Force Spectroscopy for DNA Analysis," *Biophysical Journal*, vol. 92, pp. 1632-1637, 2007.
- [14] M. A. Holden, D. Needham, and H. Bayley, "Functional Bionetworks from Nanoliter Water Droplets," *Journal of the American Chemical Society*, vol. 129, pp. 8650-8655, 2007.
- [15] M. Wiggin, "Graduate Student." The University of British Columbia, Vancouver, 2009.
- [16] Raith GmbH, "Product Information: Raith150-TWO." Germany
- [17] K. Yamazaki and H. Namatsu, "5-nm-Order Electron-Beam Lithography for Nanodevice Fabrication," *Japanese Journal of Applied Physics*, vol. 43, pp. 3767, 2004.
- [18] D. Stein, J. Li, and J. A. Golovchenko, "Ion-Beam Sculpting Time Scales," *Physical Review Letters*, vol. 89, pp. 276106, 2002.
- [19] A. J. Storm, J. H. Chen, X. S. Ling, H. W. Zandbergen, and C. Dekker, "Fabrication of solid-state nanopores with single-nanometre precision," *Nat Mater*, vol. 2, pp. 537-540, 2003.
- [20] M.-Y. Wu, D. Krapf, M. Zandbergen, H. Zandbergen, and P. E. Batson, "Formation of nanopores in a SiN/SiO₂ membrane with an electron beam," *Applied Physics Letters*, vol. 87, pp. 113106-3, 2005.
- [21] J. Li, D. Stein, C. McMullan, D. Branton, M. J. Aziz, and J. A. Golovchenko, "Ion-beam sculpting at nanometre length scales," *Nature*, vol. 412, pp. 166-169, 2001.
- [22] L. Chih Jen, A. Thomas, and B. Alexey, "Fabrication of symmetric sub-5 nm nanopores using focused ion and electron beams," *Nanotechnology*, pp. 3264, 2006.
- [23] M. J. Kim, M. D. Wanunu, C. Bell, A. Meller, "Rapid Fabrication of Uniformly Sized Nanopores and Nanopore Arrays for Parallel DNA Analysis," *Advanced Materials*, vol. 18, pp. 3149-3153, 2006.
- [24] K. Min Jun, M. Ben, M. Kazuyoshi, and M. Amit, "Characteristics of solid-state nanometre pores fabricated using a transmission electron microscope," *Nanotechnology*, pp. 205302, 2007.
- [25] W. M. Zhang, Y. G. Wang, J. Li, J. M. Xue, H. Ji, Q. Ouyang, J. Xu, and Y. Zhang, "Controllable shrinking and shaping of silicon nitride nanopores under electron irradiation," *Applied Physics Letters*, vol. 90, pp. 163102-3, 2007.

- [26] D. M. Stein, C. J. McMullan, J. Li, and J. A. Golovchenko, "Feedback-controlled ion beam sculpting apparatus," *Review of Scientific Instruments*, vol. 75, pp. 900-905, 2004.
- [27] Z. Jingmin, Y. Liping, Y. Hengqiang, and Y. Dapeng, "Fabrication of ultrafine nanostructures with single-nanometre precision in a high-resolution transmission electron microscope," *Nanotechnology*, pp. 155303, 2007.
- [28] P. Chen, T. Mitsui, D. B. Farmer, J. Golovchenko, R. G. Gordon, and D. Branton, "Atomic Layer Deposition to Fine-Tune the Surface Properties and Diameters of Fabricated Nanopores," *Nano Letters*, vol. 4, pp. 1333-1337, 2004.
- [29] C. Danelon, C. Santschi, J. Brugger, and H. Vogel, "Fabrication and Functionalization of Nanochannels by Electron-Beam-Induced Silicon Oxide Deposition," *Langmuir*, vol. 22, pp. 10711-10715, 2006.
- [30] H. P. Xinsheng S. L. Sang Ryul Park, "Fabrication of Nanopores in Silicon Chips Using Feedback Chemical Etching," *Small*, vol. 3, pp. 116-119, 2007.
- [31] Z. Siwy, D. Dobrev, R. Neumann, C. Trautmann, and K. Voss, "Electro-responsive asymmetric nanopores in polyimide with stable ion-current signal," *Applied Physics A: Materials Science & Processing*, vol. 76, pp. 781-785, 2003.
- [32] P. Y. Apel, Y. E. Korchev, Z. Siwy, R. Spohr, and M. Yoshida, "Diode-like single-ion track membrane prepared by electro-stopping," *Nuclear Instruments and Methods in Physics Research Section B: Beam Interactions with Materials and Atoms*, vol. 184, pp. 337-346, 2001.
- [33] C. Dekker, "Solid-state nanopores," *Nat Nano*, vol. 2, pp. 209-215, 2007.
- [34] S. D. Allen, T. M. Luebke, and S. D. Ross, "Ultramers™ - The Longest Oligonucleotides Available with Mass Spectrometry QC," Integrated DNA Technologies, Technical report 2007.
- [35] A. J. Storm, J. H. Chen, H. W. Zandbergen, and C. Dekker, "Translocation of double-strand DNA through a silicon oxide nanopore," *Physical Review E*, vol. 71, pp. 051903, 2005.
- [36] R. F. Egerton, P. Li, and M. Malac, "Radiation damage in the TEM and SEM," *Micron*, vol. 35, pp. 399-409, 2004.
- [37] R. F. Egerton, F. Wang, and P. A. Crozier, "Beam-Induced Damage to Thin Specimens in an Intense Electron Probe," *Microscopy and Microanalysis*, vol. 12, pp. 65-71, 2006.

- [38] C. R. Bradley, "Calculations of atomic sputtering and displacement cross-sections in solid elements by electrons with energies from threshold to 1.5 MV," 1988, pp. Medium: X; Size: Pages: 460.
- [39] FEI Company, "Product Information: Tecnai™ G² F20," vol. 00DS-TE0112. Oregon, USA, 2007.
- [40] FEI Company, "FEI Tecnai™ G² F20 Manual."
- [41] M. De Graef, *Introduction to Conventional Transmission Electron Microscopy*. Cambridge, U.K. ; New York, N.Y.: Cambridge University Press, 2003.
- [42] C. C. Striemer, T. R. Gaborski, J. L. McGrath, and P. M. Fauchet, "Charge- and size-based separation of macromolecules using ultrathin silicon membranes," *Nature*, vol. 445, pp. 749-753, 2007.
- [43] W. DeSorbo, "Ultraviolet effects and aging effects on etching characteristics of fission tracks in polycarbonate film," *Nucl. Track 3*, vol. Vol. 3, pp. pp. 13–32, 1979.
- [44] F. N. Hooge, "1/f Noise Sources," in *Advanced Experimental Methods For Noise Research in Nanoscale Electronic Devices*, 2005, pp. 3-10.
- [45] R. A. Levis, J. L. Rae, and P. M. Conn, "Low-noise patch-clamp techniques," in *Methods in Enzymology*, vol. Volume 293: Academic Press, 1998, pp. 218-266.
- [46] P. Horowitz and W. Hill, "The Art of Electronics", Cambridge University Press, 1981.
- [47] A. McWhorter, "1/f Noise and related surface effects in germanium ", vol. PhD. Cambridge, MA: Massachusetts Institute of Technology 1955.
- [48] P. G. Collins, M. S. Fuhrer, and A. Zettl, "1/f noise in carbon nanotubes," *Applied Physics Letters*, vol. 76, pp. 894-896, 2000.
- [49] U. F. Keyser, B. N. Koeleman, S. van Dorp, D. Krapf, R. M. M. Smeets, S. G. Lemay, N. H. Dekker, and C. Dekker, "Direct force measurements on DNA in a solid-state nanopore," *Nat Phys*, vol. 2, pp. 473-477, 2006.
- [50] Z. Siwy and A. Fuliński, "Origin of 1/f alpha Noise in Membrane Channel Currents," *Physical Review Letters*, vol. 89, pp. 158101, 2002.
- [51] R. M. M. Smeets, U. F. Keyser, M. Y. Wu, N. H. Dekker, and C. Dekker, "Nanobubbles in Solid-State Nanopores," *Physical Review Letters*, vol. 97, pp. 088101, 2006.

- [52] Dow Corning Corporation, "Product Information: Sylgard® 184 Silicone Elastomer," in *Silicones and Electronics*, vol. Form No. 10-898G-01. USA, 2008.

APPENDIX A: SIGNAL-TO-NOISE RATIO SCALES WITH THE NUMBER OF NANOPORES

The signal-to-noise ratio for nanopore force spectroscopy is dependent on the number of nanopores on a single membrane and the concentration of the analyte. The derivation below relates these variables and displays the potential to detect unamplified genomic DNA.



Using a first order kinetic reaction process with a rate constant k , the rate of hybridization can be related to the concentration of the analyte as follows:

$$\frac{\partial P_{hyb}}{\partial t} = k[C](P_{unhyb}) \quad (A.1)$$

P_{hyb} = Probability of hybridization at time t

$[C]$ = Concentration of analyte

P_{unhyb} = Probability of not being hybridized at time t ; $P_{hyb} = 1 - P_{unhyb}$

Integrating Eq. (A.1) with the boundary condition $P_{hyb} = 0$ at $t = 0$, and rearranging terms, we get:

$$P_{hyb} = 1 - e^{-k[C]t} \quad (A.2)$$

This exponential decay is clearly observed when working with multiple α -HL nanopores (see Fig A.1). This is then used to relate to signal-to-noise ratio using the following variables:

N = total number of nanopores

N_b = total number of hybridized nanopores

I_o = open pore current for a single nanopore

I_b = blocked pore current for a single nanopore

$$\Delta I = (I_o - I_b)$$

I_{rms} = current noise due to a single nanopore

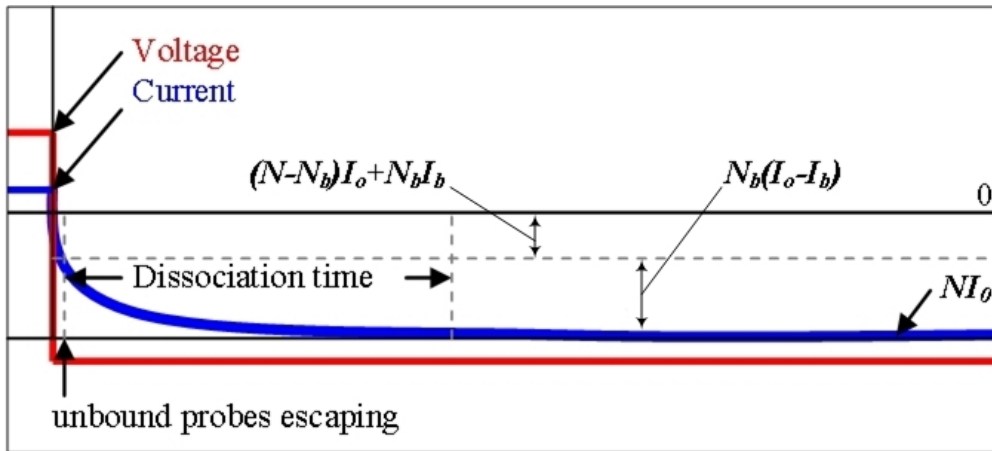


Figure A.1: Voltage and current vs. time diagram depicting the exponential decay seen during multi-nanopore experiments using α -HL.

Here, the signal is defined by the drop in current due to the total number of hybridized nanopores $N_b(I_o - I_b) = N_b \Delta I$ and the noise is

$I_{rms} \sqrt{N}$. Therefore,

$$SNR = \frac{N_b \Delta I}{I_{rms} \sqrt{N}} \quad (A.3)$$

In Eq. (A.2), P_{hyb} is the probability of hybridization or the fraction of hybridized nanopores, which is also equal to N_b/N . Using this relationship we can substitute the value of N_b in Eq. (A.3) giving us the following:

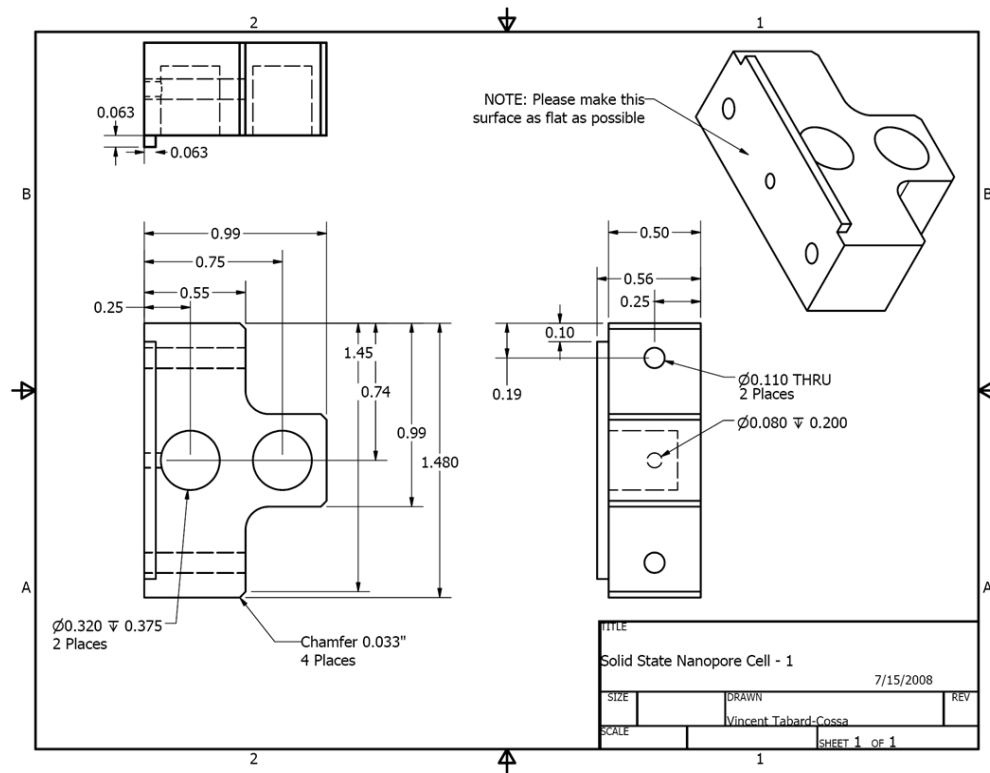
$$SNR = \frac{(1 - e^{-k[C]t}) \Delta I \sqrt{N}}{I_{rms}} \quad (A.4)$$

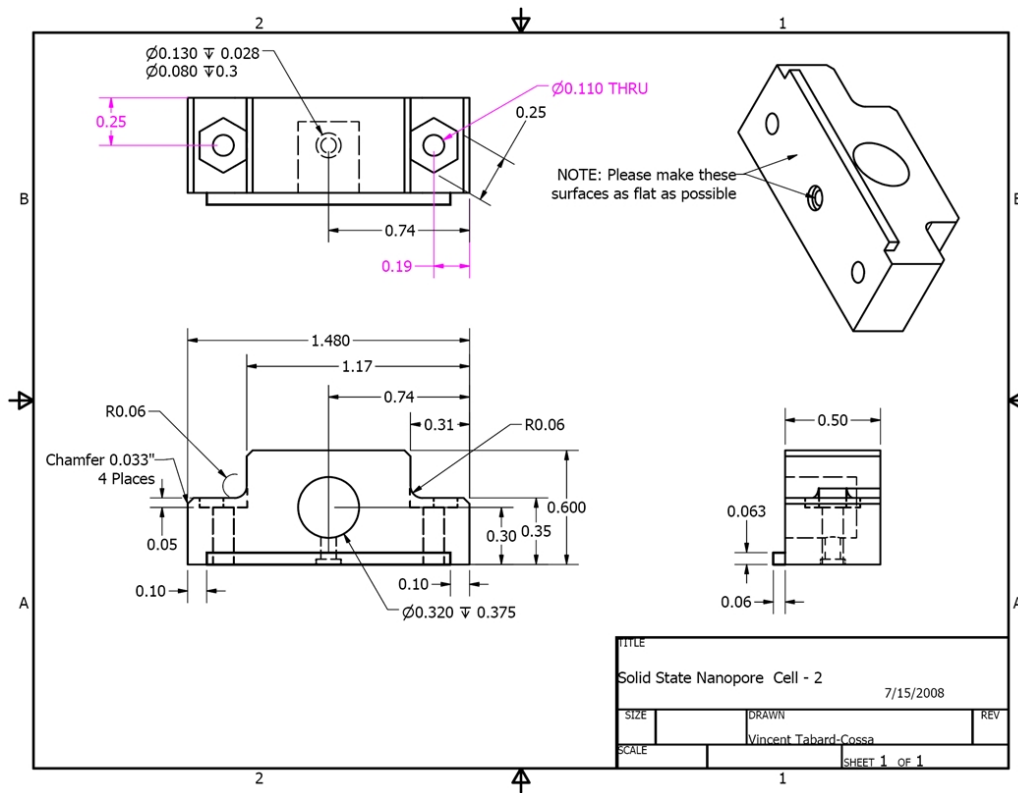
From our preliminary work on α -HL [12, 13], we can estimate the current response to be $\Delta I \sim 20$ pA at 50 mV and the value of $k \sim 10^7 \text{ M}^{-1}\text{s}^{-1}$. The associated I_{rms} in the bandwidth defined by $10 \times 1/\text{dissociation time}$, i.e. ~ 10 Hz, will be dominated by thermal noise and which can be estimated to be ≤ 100 fA. For an array element composed of 10^6 pores (which has a total resistance of $\sim 100 \Omega$), a SNR of 100 requires 500 pores to be matched with an analyte; which can be achieved in ~ 100 s at a 0.5 pM analyte concentration or at < 20 mins for a 50 fM concentration (using Eq. A.4).

Ultimately, an array of 10^6 pores has the potential of detecting femtomolar concentration in a few minutes, which means that this technique has the potential of rapidly detecting nucleotide sequence variation in unamplified genomic DNA.

APPENDIX B: DIMENSIONED DRAWINGS

B.1 Nanopore Cell





B.2 Cell Housing Assembly

